PNNL- 25781

Pacific Northwest
NATIONAL LABORATORY

Proudly Operated by Battelle Since 1965

The Effect of Rolling As-Cast and Homogenized U-10Mo Samples on the Microstructure Development and Recovery Curves

July 2016

VV Joshi
CA Lavender
DM Paxton
DE Burkes

U.S. DEPARTMENT OF ENERGY

Prepared for the U.S. Department of Energy
under Contract DE-AC05-76RL01830

DISCLAIMER

PACIFIC NORTHWEST NATIONAL LABORATORY
operated by
BATTELLE
for the
UNITED STATES DEPARTMENT OF ENERGY
under Contract DE-AC05-76RL01830

Printed in the United States of America

Available to DOE and DOE contractors from
the Office of Scientific and Technical
Information,
P.O. Box 62, Oak Ridge, TN 37831-0062
www.osti.gov
ph: (865) 576-8401
fox: (865) 576-5728
email: reports@osti.gov

Available to the public from the National Technical Information Service
5301 Shawnee Rd., Alexandria, VA 22312
ph: (800) 553-NTIS (6847)
or (703) 605-6000
email: info@ntis.gov
Online ordering: http://www.ntis.gov

PNNL-25781

The Effect of Rolling As-Cast and Homogenized U-10Mo Samples on the Microstructure Development and Recovery Curves

VV Joshi
CA Lavender
DM Paxton
DE Burkes

July 2016

Prepared for the U.S. Department of Energy
under Contract DE-AC05-76RL01830

Pacific Northwest National Laboratory
Richland, Washington 99352

Executive Summary

Over the past several years Pacific Northwest National Laboratory (PNNL) has been actively involved in supporting the U.S. Department of Energy National Nuclear Security Administration Office of Material Management and Minimization (formerly Global Threat Reduction Initiative). The U.S. High-Power Research Reactor (USHPRR) project is developing alternatives to existing highly enriched uranium alloy fuel to reduce the proliferation threat. One option for a high-density metal fuel is uranium alloyed with 10 wt% molybdenum (U-10Mo). Forming the U-10Mo fuel plates/foils via rolling is an effective technique and is actively being pursued as part of the baseline manufacturing process. The processing of these fuel plates requires systematic investigation/understanding of the pre- and post-rolling microstructure, end-state mechanical properties, residual stresses, and defects, their effect on the mill during processing, and eventually, their in-reactor performance.

In the work documented herein, studies were conducted to determine the effect of cold and hot rolling the as-cast and homogenized U-10Mo on its microstructure and hardness. The samples were homogenized at 900°C for 48 h, then later annealed for several durations and temperatures to investigate the effect on the material's microstructure and hardness. The rolling of the as-cast plate, both hot and cold, was observed to form a molybdenum-rich and -lean banded structure. The cold rolling was ineffective, and in some cases exacerbated the as-cast defects. The grains elongated along the rolling direction and formed a pancake shape, while the carbides fractured perpendicularly to the rolling direction and left porosity between fractured particles of UC. The subsequent annealing of these samples at sub-eutectoid temperatures led to rapid precipitation of the $\alpha+\gamma'$ lamellar phase, mainly in the molybdenum-lean regions. Annealing the samples above the eutectoid temperature did not refine the grain size or the banded microstructure. However, annealing the samples led to quick recovery in hardness as evidenced by a drop in Vickers hardness of 20%.

Hot rolling was performed at 650 and 800°C. The hot-rolling mill loads (load separation force) were approximately 40 to 50% less than the cold-rolling for the same reduction and thickness. It was observed that hot rolling the samples with 50% or more reduction in thickness were responsible for dynamic recrystallization in the hot-rolled samples and led to grain refinement. Unlike the cold-rolled samples, the hot-rolled samples did not fracture the carbides and appeared to heal the casting defects. The recovery phenomenon was similar to the cold-rolled samples above the eutectoid temperatures, but owing to the refined grain size, the precipitation of the $\alpha+\gamma$ lamellar phase was far more rapid in these samples and the hardness increased more rapidly than in the cold rolled sample when heated below the eutectoid temperature.

The data generated from these rolling efforts has been used to make the process modeling efforts more robust and applicable to all USHPRR partner rolling mills. The flow stress for cold rolling the samples was determined to be between 170-190 ksi, with co-efficient of friction between 0.2 and 0.4 for the PNNL mill. The measured roll separation forces and those simulated using finite element methods for hot and cold rolling for the PNNL rolling mill were in good agreement.

Acknowledgments

This work was funded by the U.S. Department of Energy and the National Nuclear Security Administration under the Office of Material Management and Minimization Reactor Conversion and performed at Pacific Northwest National Laboratory (PNNL) under contract DE-AC05-76RL01830. The authors would like to recognize the technical support in material handling and sample preparation by Mike Dahl, Karl Mattlin, Anthony Guzman, Levi Gardner, and Crystal Rutherford. In addition, the authors acknowledge Alan Schemer-Kohrn and Dan Edwards for their expertise in electron microscopy and elemental spectroscopy analysis. As indicated in the report, the experimental casting work was performed at the Y-12 Security Complex and shipped to PNNL for characterization.

Contents

Figures

Tables

Acronyms and Abbreviations

°C	degree(s) Celsius
µm	micron(s)
BSE	backscattered electron
BWXT	BWX Technologies
Cu	copper
DRX	dynamic recrystallization
EDS	energy-dispersive x-ray spectroscopy
FEM	finite element modeling
g	grams
h	hour(s)
HPRR	high-performance research reactor
HV	hardness value
in.	inch(es)
ksi	kilopounds per square inch
lb	pound(s)
LEU	low-enriched uranium
LSF	load separation force
min	minute(s)
Mo	molybdenum
PNNL	Pacific Northwest National Laboratory
rpm	rotations per minute
s	second(s)
SEM	scanning electron microscopy
U-10Mo	uranium alloyed with 10 wt% molybdenum
USHPRR	United States High-Power Research Reactor
Zr	zirconium

1.0 Introduction

In support of the U.S. Department of Energy National Nuclear Security Administration Office of Material Management and Minimization (formerly Global Threat Reduction Initiative), the Pacific Northwest National Laboratory (PNNL) has been investigating manufacturing processes for uranium-10% molybdenum (U-10Mo) alloy plate-type fuel. U-10Mo in low ^{235}U enrichments (low-enriched uranium [LEU]) has been identified as the most promising alternative to the current highly enriched uranium used in the United States' fleet of high-performance research reactors (HPRRs). The nominal configuration of the low enriched U-10Mo plate-type fuel shown in Figure 1 is comprised of a metallic U-10Mo fuel foil enriched to slightly less than 20% ^{235}U, a thin Zr interlayer-diffusion barrier, and a relatively thick outer clad of 6061 aluminum. This configuration will require the use of processes and materials not currently in use for high-enriched fuel manufacturing at BWX Technologies (BWXT, the planned manufacturer of the low-enriched fuel)), so the USHPRR project is investigating several thermomechanical processing techniques to rapidly determine the most cost-effective and robust method for manufacturing the plate fuel (Burkes and Senor 2014; Senor and Burkes 2014).

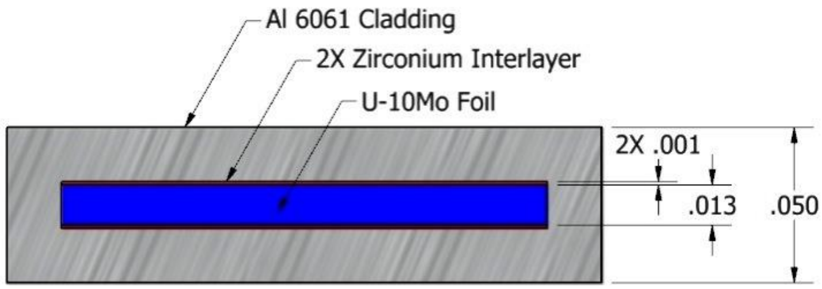

Figure 1. Nominal As-Bonded Geometry of the HPRR U-10Mo Fuel Prior to Final Shaping. (Dimensions are in inches).

Rolling of foils from a cast slab is one such effective technique used to form the reactor plates and is being implemented in BWXT production (Burkes et al. 2010; Senor and Burkes 2014; Park et al. 2014). The thermomechanical processing of U-10Mo directly correlates with the structures/phases formed. Earlier work by Burkes et al. (2009, 2010) had shown that 0.01" thick foils rolled from the 0.125" thick as-cast coupon at 650°C exhibited a banded microstructure. The (as-rolled) foils annealed at 650°C for 0.5 and 1 h and at 675°C for 2 h showed an increase in both Young's modulus and 0.2% offset yield strength. Increased annealing duration of the alloys resulted in higher ultimate tensile strengths and was proportional to the degree of molybdenum (Mo) homogenization. More recent work on the fabrication of U-10Mo has focused on understanding the interface with the cladding materials (Perez et al. 2010; Park et al. 2014, 2015). Despite the progress and a modest amount of published literature, a systematic investigation on the effects of rolling under different conditions on the microstructure development is still lacking.

Different thermomechanical processing steps lead to different microstructures (which lead to different in-reactor fuel performance), manufacturing process robustness, and manufacturing yields. Ideally, the rolling process will be optimized to address each of these technical issues. As illustrated in Figure 2, optimization requires that undesirable microstructures are avoided that desirable microstructure features are produced, Alteration of the processing parameters leads to certain advantages and disadvantages such as overall process robustness and yield and calls for an optimal solution to address all of the technical issues. Therefore it becomes pertinent to encompass all the necessary parameters, such as effect of rolling an as-cast structure, homogenized samples, rolling technique (hot/cold, reduction ratios, mill requirements, etc.) in order to understand the thermomechanical processing by rolling on U-10Mo. The challenges that need to be addressed here are creating a desirable microstructure that improves yield and determine the defects that may occur as function of rolling reductions, temperature and number of passes as described in Figure 2 and at the same time determine the time and temperature required to anneal the microstructure for further processing

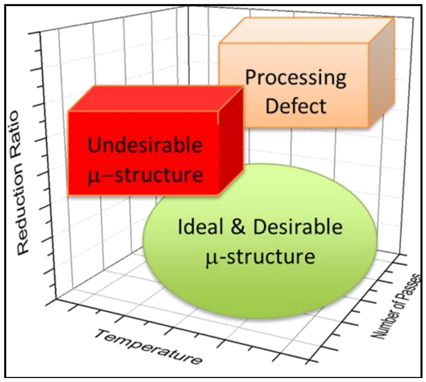

Figure 2. Effect of Thermomechanical Processing Parameters on Producing a Defect-Free/Desirable Microstructure

Experimental investigations will differ widely with rolling mills and associated configurations, such as roll diameter and speed. In order to eliminate any discrepancies in the rolling studies performed and allow the successful transfer of technology to BWXT, it becomes imperative to develop a robust modeling technique that can predict the material behavior in different mills and under different conditions. The modeling work (Soulami et al. 2014) currently being conducted at PNNL uses finite element modeling (FEM) simulations to predict the roll-separating force and the rolling defects. Eventually, this technique combined with microstructure-based modeling, can reliably predict the microstructure and other related processing phenomena. In order to make the models more robust and to verify their results, they need to be complemented by experimental studies.

Based on the previous work mentioned above, a systematic study on interrupted rolling (e.g., rolling studies examining a portion of the overall rolling schedule) should address the effects of:

- rolling the as-cast and homogenized U-10Mo on the microstructure and mechanical properties and the defects associated with them
- hot and cold rolling and reduction ratios, and combinations of the same, on the microstructure and mechanical properties and the defects associated with them.

These studies should be used to provide a feedback loop to the ongoing FEM as well as the reactor performance modeling being conducted at PNNL, and eventually lead to development of a processing window where the process produces high yields of consistent, high-performing foils. The processing window developed will focus on conditions required to obtain defect-free processing as a function of number of rolling passes, reduction ratio, and temperature.

In the current work, as-cast U-10Mo plates of thicknesses 0.2 in. and 0.375 in. were cut into samples and used for the interrupted rolling studies. The current work focuses on systematically investigating the correlation between bare rolling and the mill parameters and sample geometry on the microstructure development, mechanical properties, and eventually the effect of annealing on the recovery and recrystallization. Initial trials were focused on understanding the effect of a single pass on the as-cast samples and their microstructure. Later, a more detailed study was conducted to investigate the effect of hot versus cold rolling on as-cast and homogenized samples. Detailed characterization was performed before and after rolling to identify microstructural details using scanning electron microscopy (SEM) and x-ray diffraction (XRD). The post-rolling studies included studying the effect of annealing on microstructure development and the recovery curves.

2.0 Experimental

The procedure of the rolling experiments, materials used, the process baseline (PB) sample [Nyberg et. al 2013a], and characterization of the microstructure of the as-received and rolled U-10Mo samples are described below.

2.1 Rolling Equipment and Procedures

For the current work, rolling was performed on a Stanat model TA-215, two-high mill (Figure 3). The top and bottom rolls were 4 in. in diameter and roughly 8 in. wide. The rolling experiments were performed without any lubrication. To roll the depleted U-10Mo samples, the samples were wrapped in zirconium foils roughly 0.001 in. thick. The mill was operated at 25 rpm and had a maximum load separation force (LSF) of 100,000 lb. The LSF was measured using two load button cells (model LBC-50K obtained from transducertechnoligies.com) placed underneath the roller bearings. The data from the load cells were measured using two software packages: DPM-3-DLS for peak load and Personal DaqView Plus for real time load data during rolling

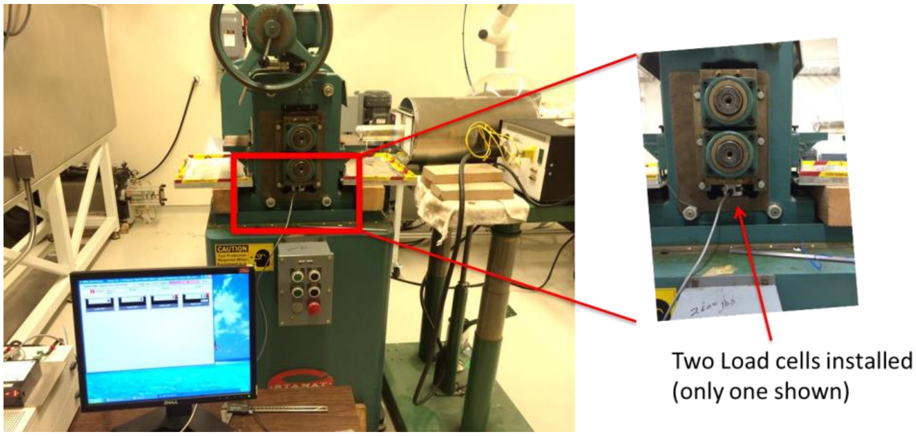

Figure 3. Side View of Stanat TA-215 Rolling Mill, with Load Cells Shown in the Inset

Under the influence of the high rolling forces the mill is elastically stretched like a spring. Because of this, the thickness of the rolled sample exiting the rolling mill is greater than the roll gap set. In order to predict the exact thickness of the rolled sheet the elastic constant of the mill is determined. Additionally, a calibration curve/elastic constant is necessary to correlate the actual rolling data with the modeling work. The elasticity of the rolling was evaluated using an Al6061-T6 sheet. The samples were rolled with different reductions to determine the mill spring within the system. Figure 4 shows the calibration curve, or a plot of load separation force (LSF) as a function of mill spring. (Dieter G.E. 1976) The mill had an elastic constant of 0.448 GN/m (2.5×10^6 lb/in.).

For hot-rolling, the samples were pre-heated in air at the required temperature for 20−30 min in a Thermcraft Model 1134 tube furnace before they were fed through the mill. The samples were immediately rolled (within 5 s) to avoid any loss of heat during the hot-rolling procedure. The annealing and homogenization of the samples was performed in an MTI model VBF-1200X-H8 furnace in a continuously flowing argon atmosphere. The samples were usually ramped up to the required temperature and cooled, at 10°C/min.

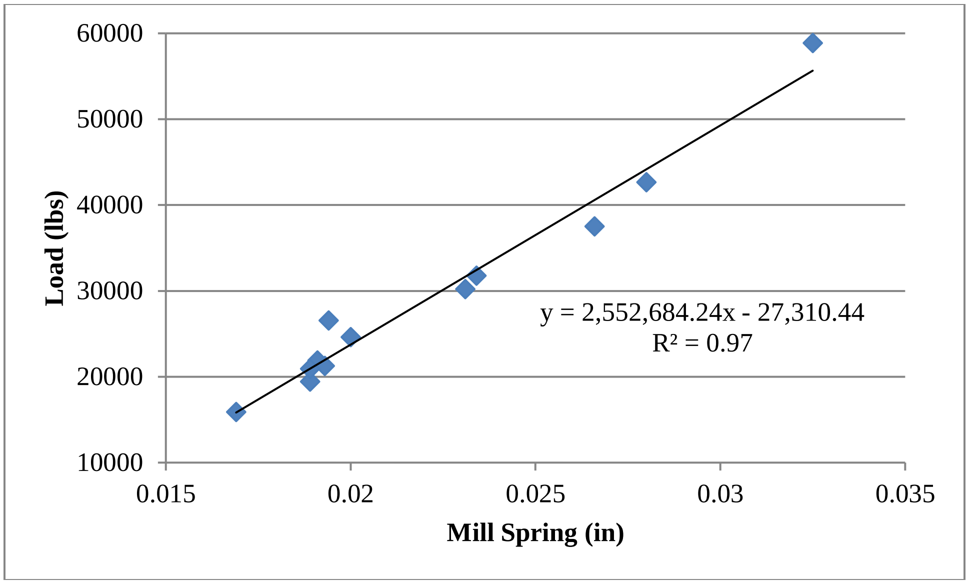

Figure 4. Calibration Curve to Determine the Elastic Constant of the Rolling Mill

For every rolling pass, the area reduction, percent spread, true strain, and lateral spread coefficient were measured as described in the equations below:

$$R = \left(\frac{t_i - t_f}{t_i}\right) \tag{1}$$

$$\epsilon = ln\left(\frac{t_i}{t_f}\right) \tag{2}$$

$$S_w = \frac{ln\left(\frac{w_f}{w_i}\right)}{\ln\left(\frac{t_i}{t_f}\right)} \tag{3}$$

where R is reduction per rolling pass; ϵ is the true strain; t_i, t_f, w_i, and w_f are the initial and final thickness and initial and final width of the samples, respectively, and S_w is the lateral width coefficient.

2.2 Materials

Two depleted U-10Mo plates were cast at the Y12 National Security Complex, in Oak Ridge, Tennessee: one 0.2 in. thick, labeled 3rd Andrew (A3), and the other 0.375 in. thick, labeled 1st Andrew (A1). These plates were 5 in. wide and 7 in. long and were cast in a book mold along the length. The gates and risers at the 5 in. section were removed and the plates were later sent to Manufacturing Sciences Corporation (now Energy Solutions, Inc.), in Oak Ridge, Tennessee for machining. Plates A3 and A1 were milled to final thicknesses of 0.148 in. and 0.329 in., respectively, and each plate was later sectioned into approximately 0.75 × 0.9 in. sample coupons, as shown in Figure 5. The plates were sectioned to totals of 88 and 36 samples from A3 and A1, respectively, as shown in Figure 5.

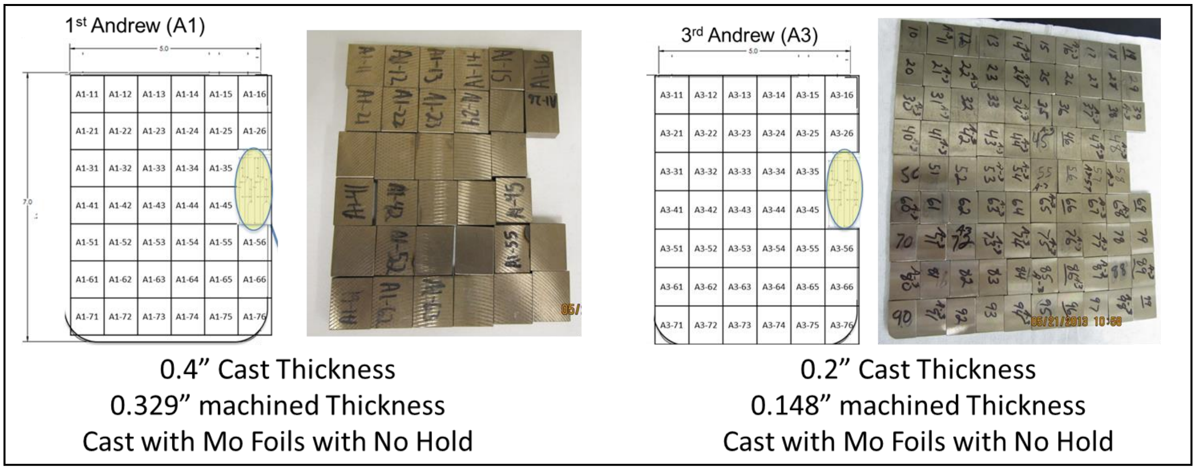

Figure 5. As-Received Samples from Y12

Due to the limited number of the samples available from A3 and A1, samples previously obtained from a process baseline (PB) study (Nyberg et al. 2013a, b) were also used for the rolling studies. The sample used for the current work was identified as 5th Matthew (YN-TW8W) and was cast into 0.2 in. thick plate. This plate was hot topped and for the current report the sample will be referred to as the process baseline (PB) sample.

2.3 Microstructural Characterization of Samples

The as-received or the rolled samples were sectioned longitudinally and were prepared for microstructural characterization. The details of the metallographic preparation can be found in a previous report (Edwards et al. 2012, Prabhakaran et. al 2015). Microstructural characterization was performed using an optical microscope as well as a JEOL JSM-7600F SEM equipped with an Oxford Instruments X-Max 80 energy-dispersive x-ray spectroscopy (EDS) detector. The EDS analysis was performed using INCA Microanalysis Suite software, version 4.15.

XRD analysis was conducted in a Rigaku Ultima IV equipped with a monochromated Cu K-α x-ray source and a linear position-sensitive silicon strip detector. In general, diffraction data were collected between 25 and 120° 2θ in 0.001° increments at a scan rate of 0.5°/min. The hardness of the polished rolled and heat-treated samples was measured using a semiautomatic Future-Tech Model FM-7 microhardness tester. The indents were made with a 500 g load at a dwell time of 15 s.

3.0 Results

The results of the microstructural characterization of the as-received material and the effects of rolling the samples are described below. This section is primarily divided into four parts: (1) characterization of the as-received material (Section 3.1), (2) the effect of hot rolling the interrupted rolling samples with a single pass (Section 3.2), (3) the effect of rolling the PB samples (hot and cold) (Section 3.3) and (4) the effect of rolling the as-cast and homogenized interrupted rolling samples, hot or cold, from 0.2 in. to 0.002 in. (Section 3.4).

3.1 Microstructural Characterization of As-Received Material

As-cast PB A1 and A3 samples were characterized as described in the following sections.

3.1.1 Characterization of Process Baseline Sample (5th Matthew 0.2 in. Sample)

Figure 6 shows the microstructures as determined by backscattered electron scanning electron microscopy (BSE-SEM) of the as-cast PB samples (i.e., YN-TW8W/5th Matthew 0:2). These castings were 8 × 9.1 in. and 8 × 8.5 in., respectively. The images correspond to the top, middle, and bottom sections of the casting. Images in Figure 6a-c were taken at 100X and images in Figure 6d-f were taken at 500X magnifications.

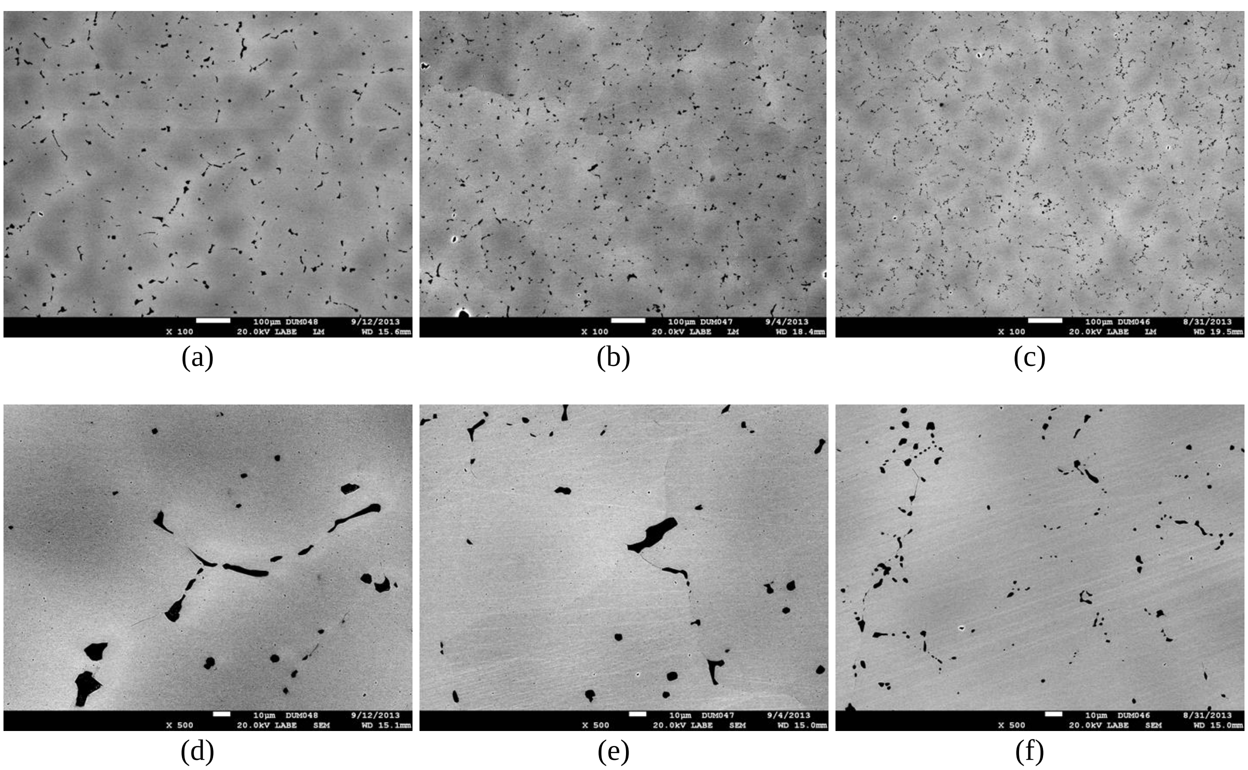

Figure 6. BSE-SEM Images of Casting 5th Matthew 0:2 (0.200 in. thick, no hold). (a,d) top, (b,e) middle, and (c,f) bottom at (a-c) 100× and (d-f) 500×

The grain size decreases at the bottom of each casting, likely corresponding to the cooler location at the bottom of the mold and faster cooling rate. Specifically, the grain size from top to bottom varied from 85 to 60 µm for sample 5th Matthew 0:2. The variation in Mo between the lean and rich regions was not detectable optically in these samples. There is slight evidence of a dendritic structure and isolated porosity observed at the dendrite interfaces, which were less than 25 µm in size. As mentioned previously, although observed in the optical image, Mo segregation was detected in the BSE-SEM images and EDS measurements. Mo segregation is evident and the variation in Mo concentration between the lean and rich regions was determined to be 1 to 2 wt%. Uranium carbides (shown as the dark particles in the BSE-SEM images) were primarily located along the grain boundaries and were elliptical in shape. The approximate area fraction of carbides calculated by ImageJ analysis was 1.7%.

3.1.2 Characterization of the As-Cast Interrupted Rolling Sample:A3 (Andrew 3rd, 0.2 in.)

The microstructure in the A3 samples varied from top to bottom. Figure 7 shows the microstructure from the top, middle, and bottom sections. The samples used here for microstructural characterization were obtained from the left edge of the A3 sample. The grain size remained consistent from top to bottom at 100−125 µm. The microstructure had a typical dendritic structure with molybdenum-rich and -lean regions. The carbide volume fractions were approximately 2.1% of the net area and were not spherical. However, an increased concentration of a non-stoichiometric oxygen-rich phase was observed from the top to the bottom of the sample. This phase had a distinctive pine/fir tree appearance.

Figure 8 shows a composite EDS map of a region in the bottom sample. These regions were rich in oxygen and lean in molybdenum. Semi-quantitative EDS analysis (Figure 8) revealed that the weight percentage of oxygen in this phase was approximately 1.5 times that of the base alloy. XRD analysis of the bottom and middle samples was conducted (Figure 9) and only peaks corresponding to γ-uranium and uranium carbide were observed, indicating presence of a non-stoichiometric phase in these samples.

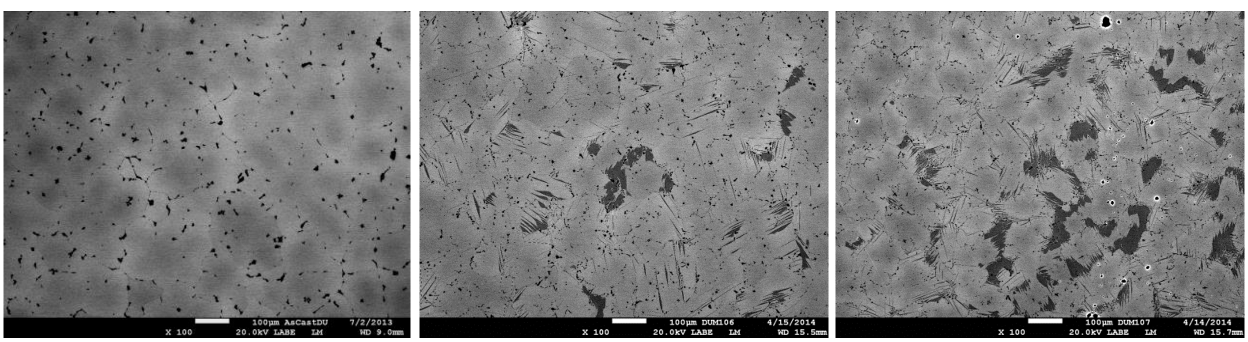

(a) (b) (c)

Figure 7. Microstructure from the (a) Top, (b) Middle, and (c) Bottom Sections of Cast Plate A3 (Andrew 3rd)

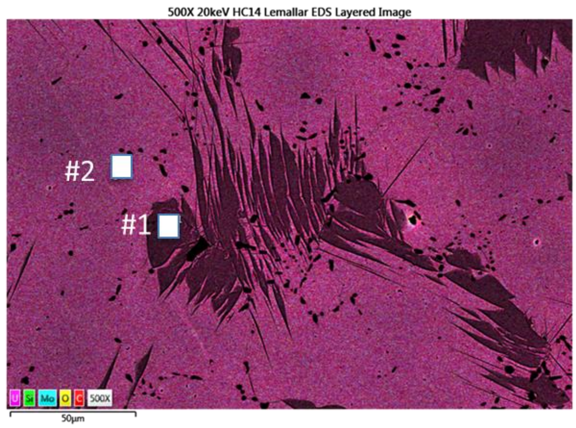

Result Type	Weight %				
Spectrum Label	O	Si	Mo	U	Total
# 1	3.22	0.11	8.82	87.86	100.00
# 2	1.86	0.12	10.26	87.77	100.00

Figure 8. Composite EDS Map and Semiquantitative Analysis of the Region in the Bottom Samples of A3 Showing the Oxygen-Rich Phase

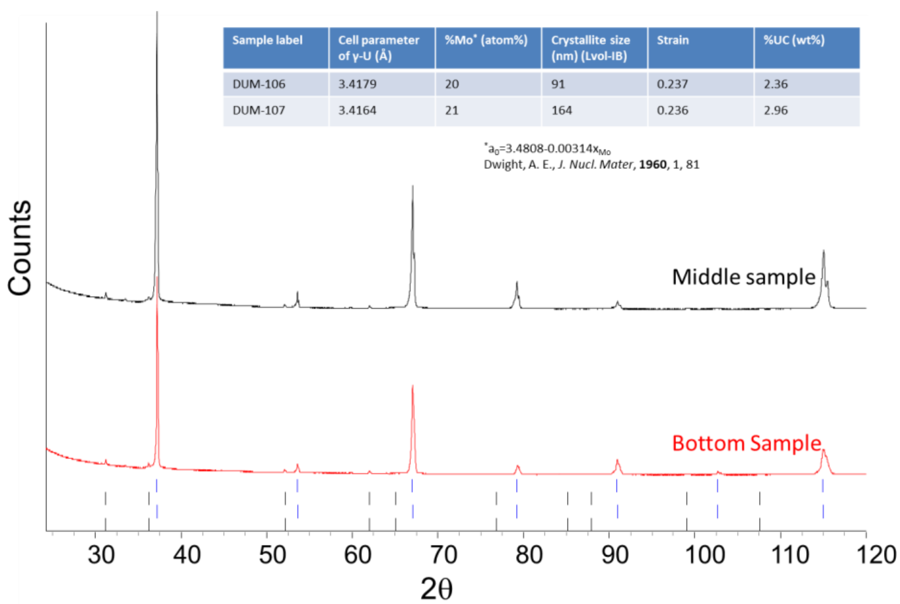

Sample label	Cell parameter of γ-U (Å)	%Mo* (atom%)	Crystallite size (nm) (Lvol-IB)	Strain	%UC (wt%)
DUM-106	3.4179	20	91	0.237	2.36
DUM-107	3.4164	21	164	0.236	2.96

*a_0=3.4808-0.00314x_{Mo}
Dwight, A. E., *J. Nucl. Mater*, **1960**, 1, 81

Figure 9. XRD Analysis of the Middle and the Bottom Samples from A3. The black vertical lines correspond to carbide phase and blue vertical lines correspond to the γ-uranium phase.

3.1.3 Characterization of the As-Cast Interrupted Rolling Sample: A1 (Andrew 1st, 0.375 in.)

Figure 10 is the longitudinal cross-section BSE-SEM image from the top region of the as-cast sample of the U-10Mo sample that was cast into 0.375 in. plate and was later machined down to 0.325 in. The microstructure closely resembles the A3 samples’ top region with its dendritic structure and a molybdenum-rich and -lean microstructure. The grain boundaries were decorated with carbides and had an aspect ratio/ were elliptic in shape. The volume fraction of the carbides was approximately 2.0% of the net area. Because of the fewer number of samples available, the samples from the middle and bottom were not used for metallographic sample preparation; only samples from the top section were used for the rolling study.

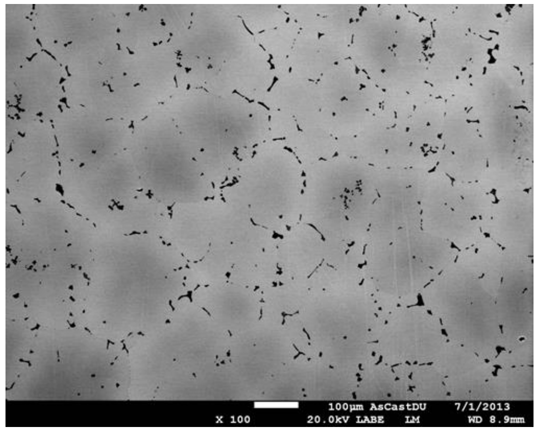

Figure 10. Microstructure from the Top Section of Sample A1 (Andrew 1st)

3.2 Effect of Rolling As Cast Samples at 800°C

The initial interrupted rolling study was focused on evaluating the effect of rolling the samples at 800°C with 10, 25, and 50% reductions. The primary goal of these investigations was to determine the minimum strain required to deform the grain size through the thickness of the sample and its effect on the microstructure and defects, if any. A temperature of 800°C was specifically chosen for this work because for any given composition of molybdenum, the sample is processed entirely in the gamma phase field and any possibility of phase precipitation in the molybdenum-lean regions is completely avoided. During the compression testing of U-10Mo (Joshi et al. 2013; Joshi et al. 2014; Nyberg et al. 2013a) it was also determined that no stress-induced phase precipitation/transformation occurs at this temperature. At the same time, a strain of 40% is responsible for partially homogenizing the sample as shown in Figure 11. The microstructure developed from these studies—including the degree of homogenization—will be compared the microstructure generated using our FEM of the rolling process.

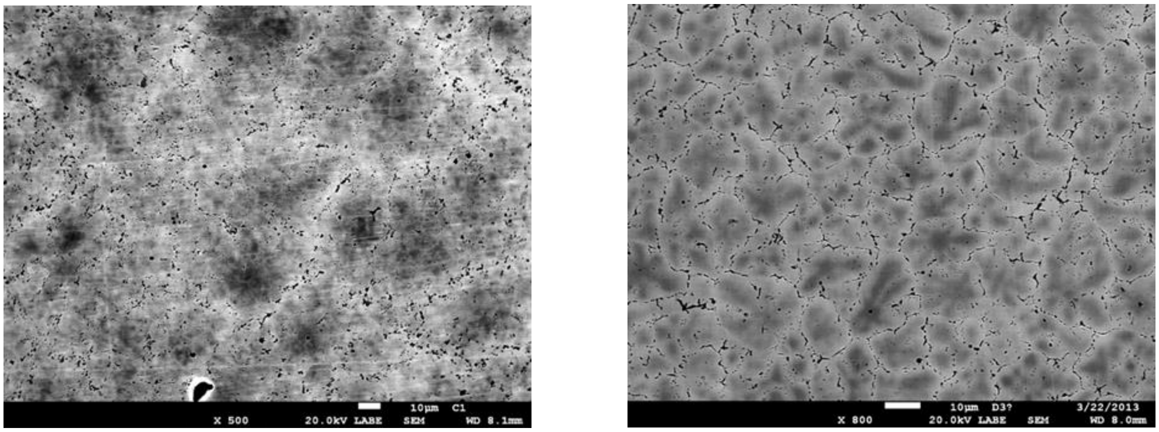

(a) (b)

Figure 11. (a) Microstructure of the As-Cast Pin Sample after Compression Testing at 800°C to a 40% Strain; (b) Microstructure after Following the Same Thermal Profile of the Sample without Any Strain

3.2.1 Rolling the A3 ~0.147 in. Samples at 800°C

The A3 0.147 in. sample underwent reductions of 10, 25, and 50% at 800°C. As described earlier, the samples were wrapped in a 0.001 in. Zr foil and were soaked at 800°C for 20 min prior to rolling; they were then rolled immediately. Figure 12a, b, and c show the effects of rolling 0.147 in. samples at 800°C with 10, 25, and 50% reductions, respectively. Table 1 shows the effects of rolling at 800°C on the rolling parameters. The calculations were made based on Equations (1)−(3). The strain rates for the rolling were 2, 4, and 5 s^{-1}, respectively for 10, 25, and 50% reductions. Owing to the buck or draft during the rolling, the samples were rolled to approximately 8, 19, and 38%, but for further discussion are still referred to as the 10, 25, and 50% reductions, respectively. The samples that had reductions of 10 and 25% rolled without any defects, whereas the sample with 50% reduction had a centerline crack, as shown in Figure 12. It was also observed that the samples underwent a large lateral spread, and the centerline cracking in the 50% reduction sample can be attributed to this phenomenon (Dieter 1976; Ginzburg 1993). In the 50% reduction sample, the sample spread approximately 11% (in the uncracked region) upon rolling, whereas in the case of 10 and 25% reductions the lateral spreads were 2 and 7%, respectively. There was no correlation between the width spread coefficient (S_w) and thickness and the crack observed.

Longitudinal cross-sectional montage images of the rolled samples are shown in Figure 12. The samples that were rolled with 10 and 25% reduction were observed to have retained their as-cast structure; i.e., the dendritic molybdenum segregated microstructure/coring structure was still retained. The carbides did not fracture and were still located at the grain boundaries, indicating the matrix was softer than the carbides at the processing temperature (Nyberg et al. 2013b). The presence of the carbides may have resulted in the pinning of the grain boundaries. However, in the case of the 50% reduction sample, the as-cast structure was completely broken down. A fibrous structure was observed with molybdenum-lean and -rich regions indicating severe deformation, similar to those observed by Burkes et al. (2010) and Park et al. (2014). The carbides were located at the grain boundaries, indicating pinning of the grain boundaries by the carbides (Rollett et al. 2004; Nyberg et al. 2013a).

Table 1. Rolling Parameters for A3 Sample

Pass	Thickness	Length	Width	Reduction Per Pass	Area Reduction % Area	Area Reduction % Per Pass	% Spread Per Pass	S_w	True Strain Per Pass
Sample A3-10 10% reduction									
0	0.148	0.946	0.734		0.10				
1	0.136	1.15	0.749	8.1	0.10	6.23	2.04	0.24	0.08
Sample A3-11 25% reduction									
0	0.147	0.948	0.723		0.10				
1	0.119	1.145	0.776	19.0	0.09	13.11	7.33	0.33	0.21
Sample A3-12 50% reduction									
0	0.148	0.949	0.724		0.10				
1	0.092	1.6	0.808	37.8	0.07	30.62	11.60	0.23	0.47

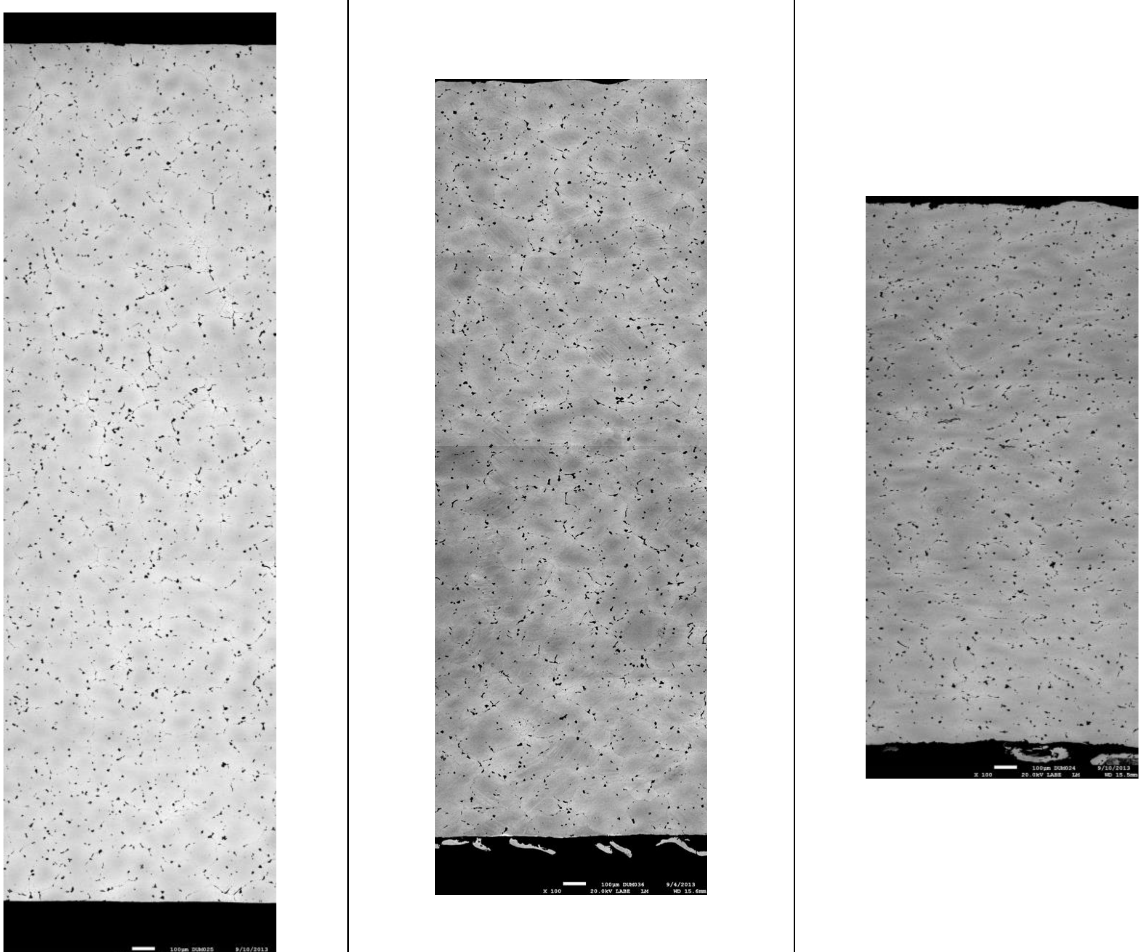

(a) (b) (c)

Figure 12. Effect of Rolling 0.147 in. U-10Mo Samples with Several Reduction Ratios. Longitudinal cross-section montage images under BSE-SEM mode for reductions of (a) 8.1%, (b) 19%, and (c) 37.8%.All the images were taken at same magnifications.

3.2.2 Rolling the A1 ~0.325 in. Samples at 800°C

Similar to the 0.147 in. samples, the A1 0.325 in. samples also underwent 10, 25, and 50% reductions at 800°C. Figure 13a, b, and c show longitudinal cross-section BSE-SEM images from the center of the rolled samples at different reductions. Table 2 describes the several rolling parameters as a function of reduction. The strain rates for the rolling were 2, 3, and 4 s^{-1} for the 10, 25, and 50% reductions, respectively. Unlike the previous sample (A3), no rolling defects were observed in the thicker samples. Owing to the buck or draft during rolling, the samples were rolled to approximately 13, 23, and 44%, respectively. Similar to the previous samples, these samples spread laterally by 2.5, 5.1, and 17%, respectively. Despite the high lateral spread in the 50% reduction sample, the sample did not crack.

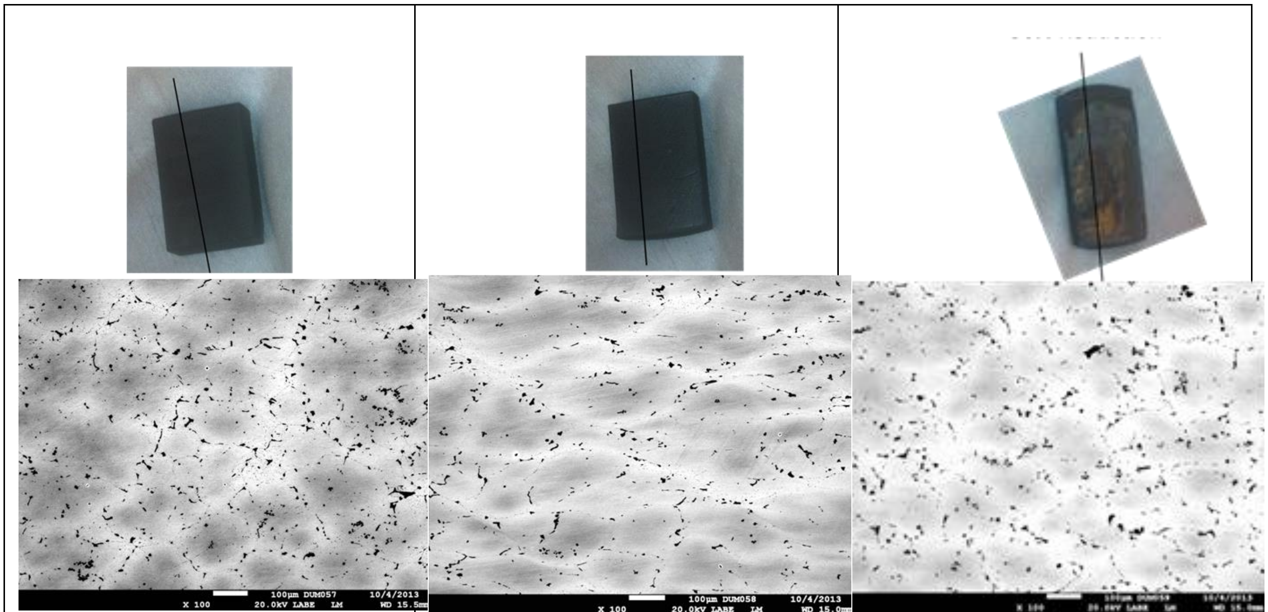

(a) (b) (c)

Figure 13. Effect of Rolling 0.325 in. U-10Mo Samples with Several Reduction Ratios. Longitudinal cross-section images at the center of the rolled samples under BSE-SEM mode for reductions of (a) 13%, (b) 23%, and (c) 44%.

Table 2. Rolling Parameters for A1 Sample

Pass	Thickness	Length	Width	Reduction Per Pass	Area Reduction % Area	Area Reduction % Per Pass	% Spread Per Pass	S_w	True Strain Per Pass
Sample A1-13 10% reduction									
0	0.329	1.05	0.746		0.24				
1	0.284	1.149	0.765	13.67	0.21	11.48	2.54	0.17	0.14
Sample A1-11 25% reduction									
0	0.325	0.995	0.795		0.25				
1	0.249	1.293	0.83	23.38	0.20	19.43	5.15	0.19	0.26
Sample A3-12 50% reduction									
0	0.324	1.14	0.754		0.24				
1	0.179	1.756	0.884	44.75	0.15	35.22	17.24	0.26	0.59

Similar to the A3 sample, the sample that underwent a reduction of 10% showed no evidence of deformation in the microstructure and the fibrous rolling texture was not visible. The dendritic structure from the cast structure was still evident. The grain sizes were between 100 and 125 μm and had an aspect ratio of 1. The carbides were still present at the grain boundaries and the microstructure was devoid of any evidence of rolling. However, rolling the as-cast billet with a 25% reduction at 800°C resulted in a rolled texture with chemical banding of molybdenum-rich and -lean regions, unlike the 0.147 in. sample in which no banding was observed. The grains were slightly elongated along the rolling direction and carbides were present at the grain boundaries. There was no evidence of cracking in the carbides, indicating the matrix was softer than the carbide phase, as was previously observed by Nyberg et al. (2013). The sample that underwent a 50% reduction showed dynamic recrystallization (DRX) with equiaxed grains of approximately 75 μm size. Molybdenum inhomogeneity was evident, but not banded as in the previous samples.

Despite the similar reductions and strain rates experienced, the microstructure varied significantly between the two samples upon rolling. There was no correlation or commonality in the two samples with regard to the width spread coefficient or percentage lateral spread. It has to be understood that the rolling is not only dependent on the mechanics of the deformation, but is also a function of microstructure or macro/micro defects and the technique employed to roll the material. Nonetheless, in the current work it was observed that rolling the as-cast U-10Mo with dendritic microstructure retains the inhomogeneity rather than eliminating it. In the thicker sample, an area reduction of approximately 50% resulted in DRX. During rolling, the matrix is softer than the carbides and does not deform or fracture the carbides. The presence of carbides at the grain boundaries will be beneficial in controlling the grain size of the final product.

3.3 Hot and Cold Rolling the Samples

Several approaches can be taken to achieve the desired foil thickness (Figure 14) and each approach provides unique challenges with regard to the final microstructure and the yield and quality of the finished product. A practical approach to rolling is to develop a test matrix and model predictions around the process/equipment limits of the manufacturer, BWXT . Based on the BWXT equipment/processing limits, we were limited to a hot-rolling temperature of 735°C due to canning in a Fe-based ca and an initial thickness of the rolling material of 0.2 in. Figure 14 illustrates the current foil process (processing routes 1 and 2) (Senor and Burkes 2014; Park et al. 2014) and the processing schedule that evaluated in the current scope of study (processing routes 3−5) with or without the homogenization heat treatment. Note that cladding of Zr foil onto the U-10Mo is of prime importance and can/cannot be incorporated into the rolling schedule. The currently used techniques are based on hot rolling the sample at 650°C, which also includes a hot roll bonding step. However, it has been determined that processing using this approach has lower yield. (Vergara et. al. 2014) Rolling, or for that matter thermomechanical processing, is a combination of processing steps. The sample can be rolled to a foil via cold rolling, a combination of hot and cold rolling, or hot and cold rolling with intermediate annealing as described in Figure 14 below.

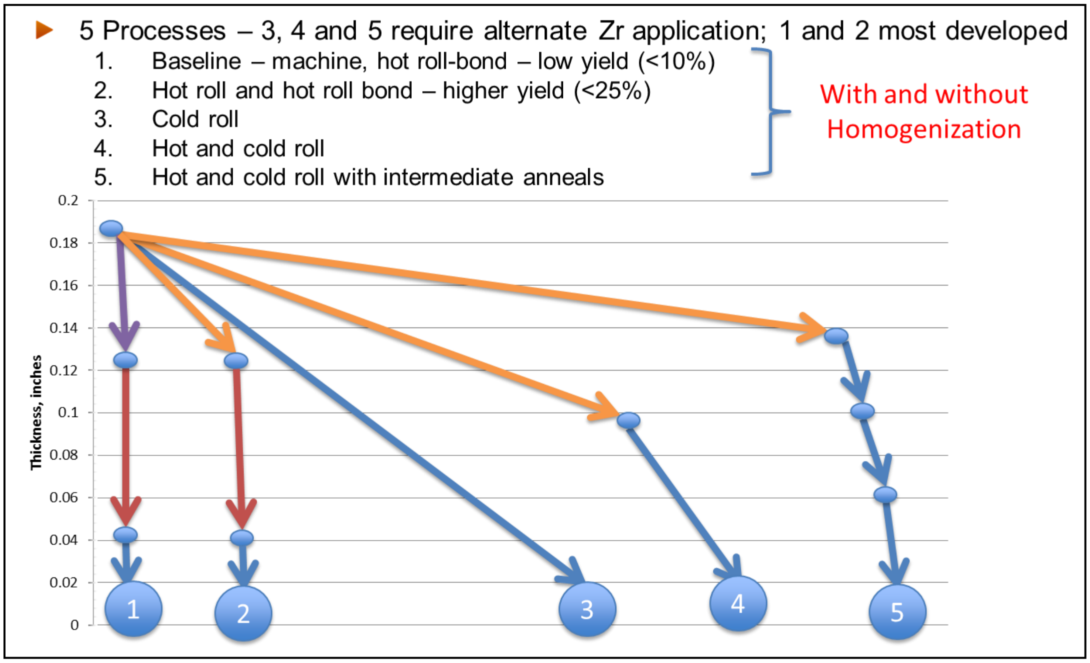

Figure 14. The Different Processing Routes Currently Used to Fabricate the U-10Mo Fuel Foil and the Proposed New Methods of Forming the Fuel Foils. Purple line: machining; red line: hot roll bonding; blue line: cold rolling; yellow line: hot rolling.

To evaluate the effects of each of these parameters, the rolling studies were specifically designed to understand the effects of each on the rolling behavior and the microstructure developed upon rolling. Because the numbers of samples available from interrupted rolling studies were fewer, PB samples were initially used to study these effects. The following processes were studied using the PB samples:

- cold rolling
- effect of homogenization on the cold rolling
- annealing/recovery curves studies
- combination of hot and cold rolling.

3.3.1 Rolling the Process Baseline Samples

The PB sample homogenization temperature and time were chosen to be 1,000°C and 4 h. The temperature and time were used to simulate the effect of hot topping on the homogenization of the castings as described in the PB study conducted previously (Nyberg et al. 2013b). The thickness and the width of the samples were not measured because they were not of uniform length (end piece of casting).

3.3.1.1 Effect of Cold Rolling the As-Cast Process Baseline Samples

The middle section (see Figure 6b, e) of the PB sample was cold rolled from 0.2 in. to 0.106 in. thick with 10% reduction per rolling pass; a total of five passes were made. The average LSF was 38,000 lb with a 0.036 in. buck. The sample did not show any signs of cracking after rolling. Figure 15 shows the longitudinal cross section of the rolled sample. Cold rolling did not eliminate the molybdenum inhomogeneity and caused the formation of molybdenum-rich and -lean bands. It was also observed that cold rolling was ineffective in closing the as-cast porosity and elongated it along the rolling direction (Figure 15a). The carbides (Figure 15b) fractured perpendicularly to the rolling direction (Tabei and Garmestani 2013). It appeared that rolling caused porosity to form in the fractured zone.

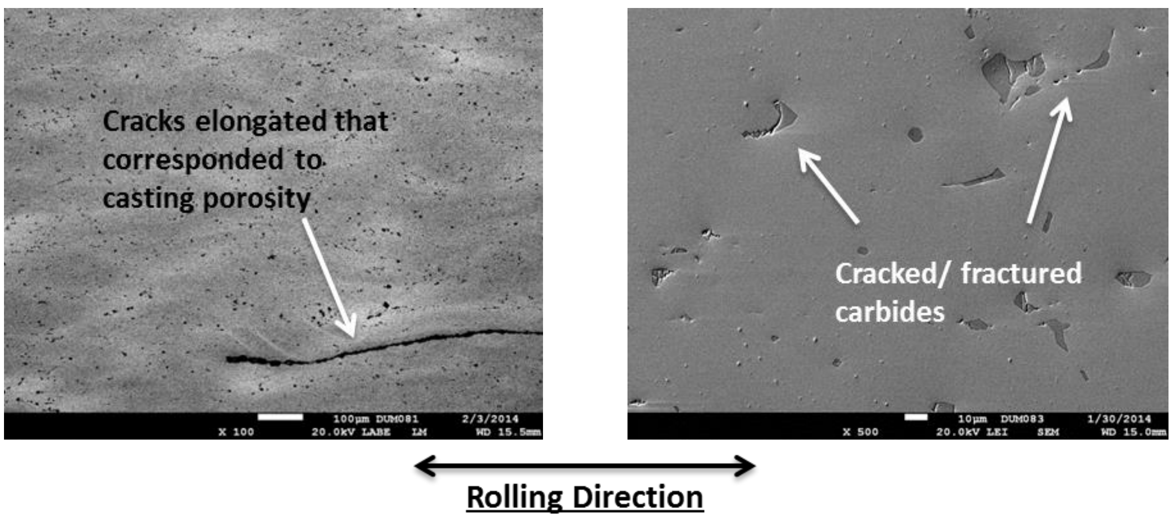

(a) (b)

Figure 15. SEM Images Showing the Effect of Cold Rolling the As-Cast PB Samples on the Microstructure Development: (a) elongation of the casting porosity and (b) cracks in the carbide perpendicular to the rolling direction.

After rolling, the samples were subjected to a homogenization heat treatment at 1,000°C for 4 h to observe the homogenization behavior of the samples. The homogenization heat treatment was ineffective in eliminating the molybdenum inhomogeneity (Figure 16) and the sample had a hardness of 280 HV.

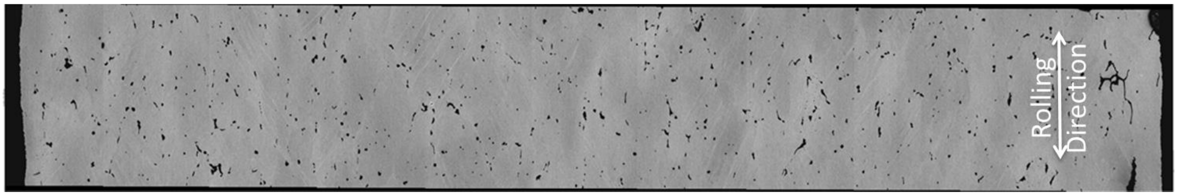

Figure 16. PB Sample after Homogenization at 1,000°C for 4 h

To determine the recovery and recrystallization behavior, the samples were heat treated at 500, 650, and 800°C for several durations. Figure 17 shows the effect of heat treatment on the sample hardness as a function of time and Figure 18 shows the resulting representative microstructures. Heating the samples above the eutectoid temperature has an immediate effect on the hardness, and the hardness remains constant even after several durations at the given temperature. The hardness of these samples was above those of the 1,000°C-4 h samples. Heating the samples below the eutectoid temperature led to an initial drop in the hardness, but the hardness later increased as a result of the precipitation of the lamellar phase, as shown in Figure 18a. Annealing led to immediate recovery of the stresses and further annealing did not significantly improve the hardness above the eutectoid temperature. No evidence of grain growth/recrystallization was observed in the annealed samples.

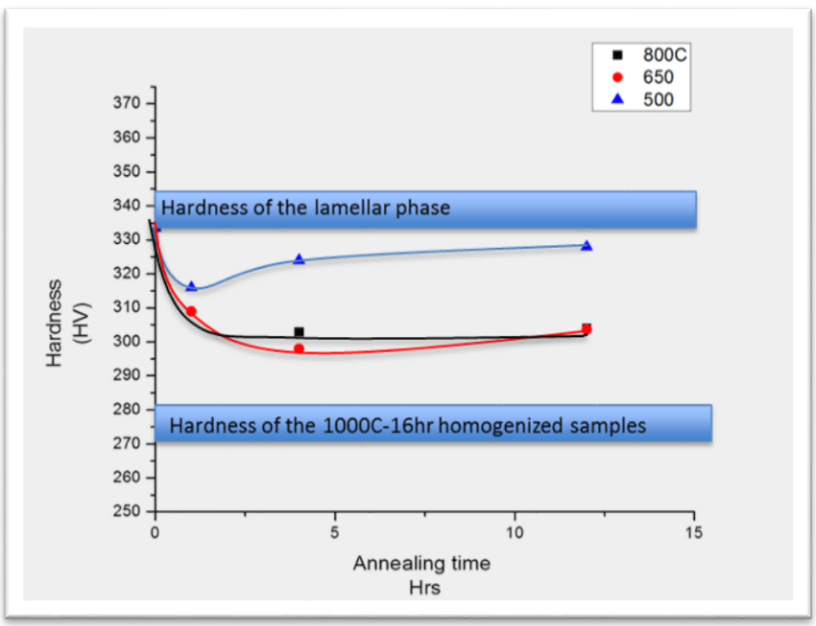

Figure 17. Effect of Annealing at Several Times and Temperatures on the As-Cast Rolled PB Sample

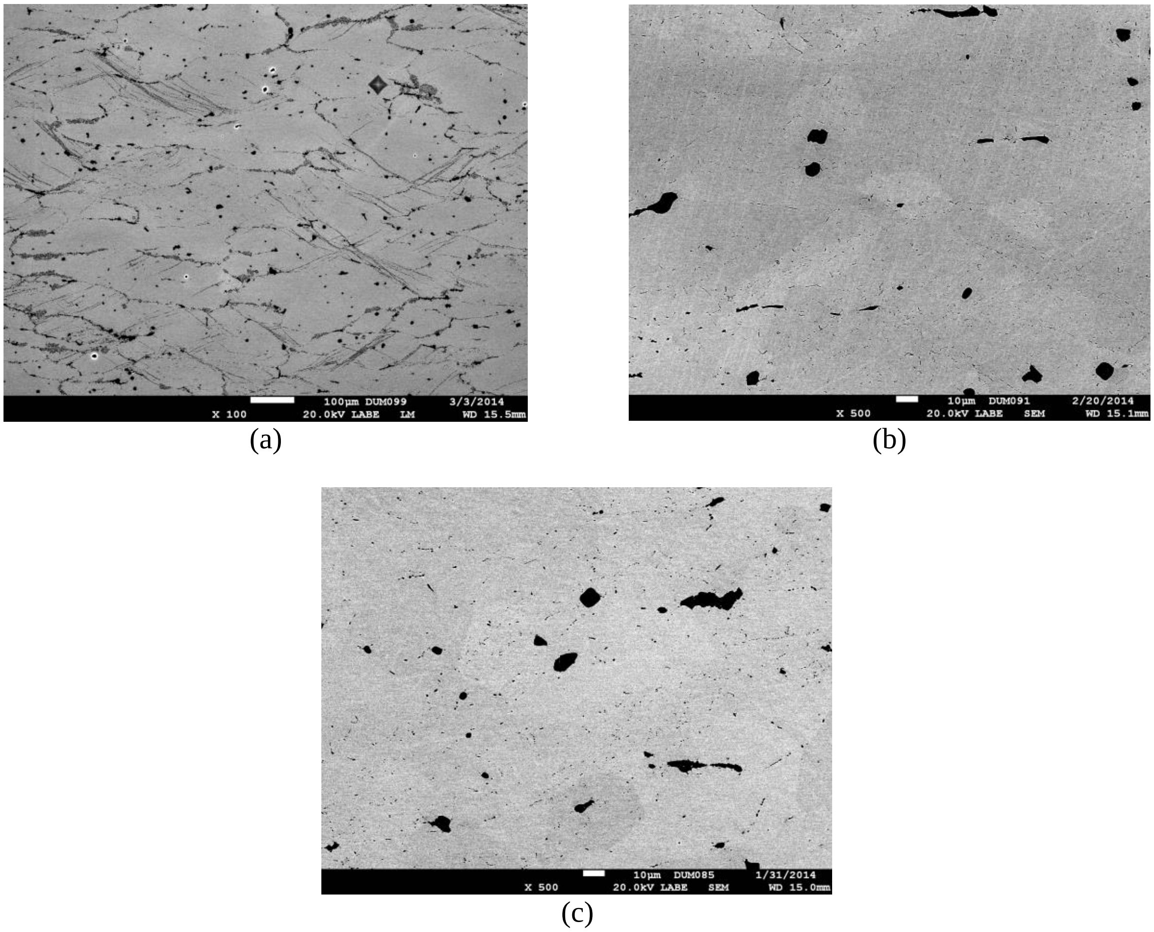

Figure 18. BSE-SEM Images of the As-Cast, Rolled PB Samples after 12 h of Annealing at (a) 500, (b) 650, and (c) 800°C

3.3.1.2 Effect of Cold Rolling the 1,000°C-4 h Annealed Process Baseline Samples

The top and the bottom sections of the PB samples were annealed at 1,000°C for 4 h to simulate the hot topping behavior and then rolled similarly to the as-cast PB sample. There was no evidence of cracking upon rolling. The LSFs were similar to those for previous PB samples. After rolling, the image of the longitudinal cross section revealed a banded microstructure similar to that of the as-cast, rolled PB sample. The carbides fractured perpendicularly to the rolling direction. The cold rolling was not helpful in closing the existing porosity (Figure 19).

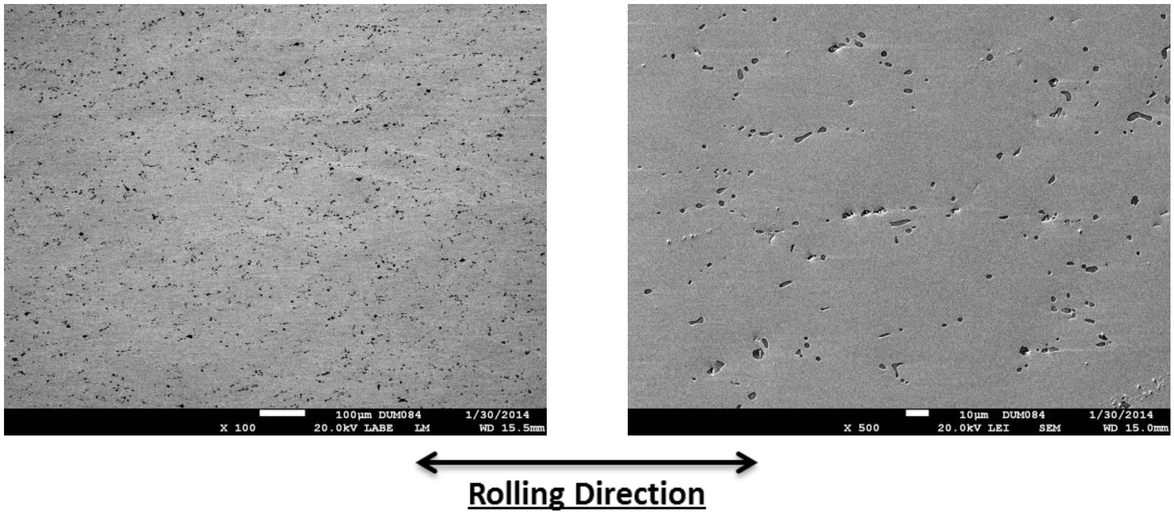

(a) (b)

Figure 19. BSE-SEM Images Showing the Effect of Cold Rolling the PB Samples Annealed at 1,000°C for 4 h on the Microstructure Development. Image (b) is a magnified image of a region shown in (a).

Annealing the samples below and above the eutectoid temperature yielded similar hardness phenomena (Figure 20). However, in this case the as-rolled hardness was less than the previous ones, and the drop in hardness was not as pronounced as that observed in the previous samples. Figure 21 shows the BSE-SEM image of the annealed samples. Sub-eutectoid annealing led to precipitation of the lamellar phase primarily along the grain boundaries (Figure 21c), whereas the samples annealed above the eutectoid temperature did not show any significant recrystallization or grain growth.

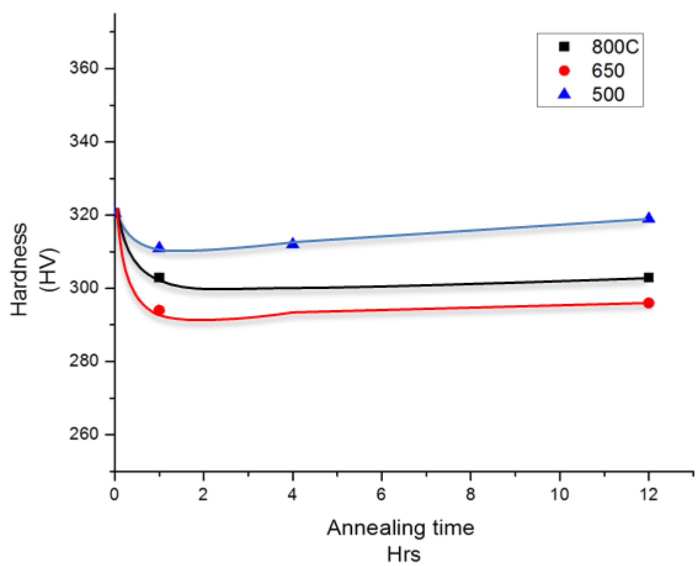

Figure 20. Effect of Annealing at Several Times and Temperatures on the PB Sample Rolled after Previous Annealing at 1,000°C for 4 h

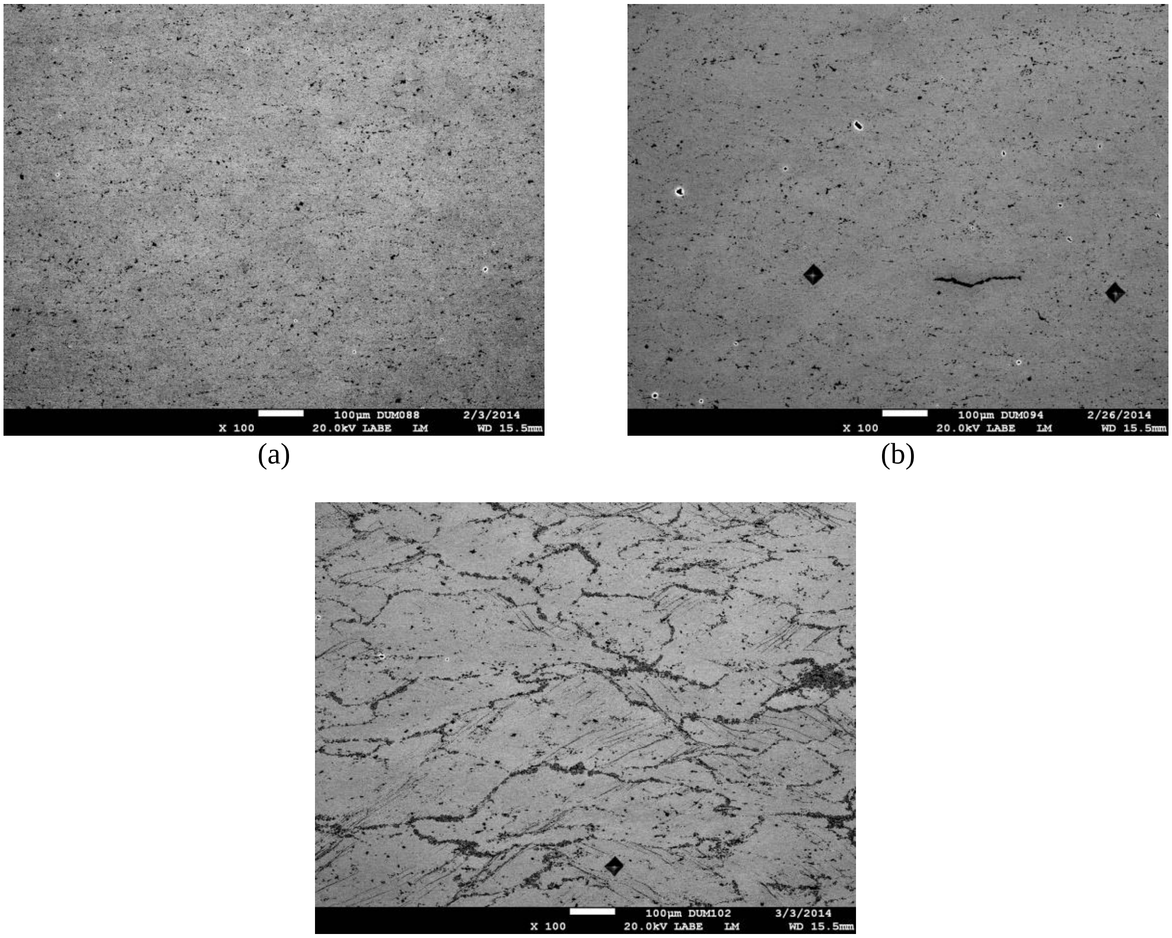

(a) (b)

(c)

Figure 21. BSE-SEM Images of the 1,000°C-4 h Annealed, Rolled PB Samples after 12 h of Annealing at (a) 800, (b) 650, and (c) 500°C

3.3.2 Rolling the Interrupted Rolling Samples

The effect of rolling using proposed different processing routes (Figure 14) on defect formation and microstructure development were studied to define the ideal path for rolling the material. In addition, the rolling parameters were fed into the modeling studies to make the models more robust. The effects of hot and cold rolling as-cast and homogenized samples were investigated. The samples from both top and bottom sections of the A3 (Andrew 3rd) cast plate (see Figure 7) were investigated for repeatability of the process. For the current study, the selected homogenization temperature and time were 900°C for 48 h.

3.3.2.1 Effect of Cold Rolling A3 Samples

A3 samples were cold rolled from 0.147 in. to 0.02 in., with 10% reduction per rolling pass, using 4 in. rolls, as described previously. No intermediate annealing or trimming of the rolling samples were performed.

Table 3 shows the cold-rolling data from the top section of the A3 plate (see Figure 7). Slight edge cracking was observed on the ninth pass (highlighted in red) as the samples were rolled, but further rolling of the samples resulted in containment of the cracks. Figure 22 shows the sample after achieving a final thickness of 0.02 in.

Table 3. Rolling Data to Study the Effect of Location on Cold Rolling: Top of the Plate Sample (A3-24), As Cast

Sample A3-24 cold rolling												
Pass	Thickness	Length	Width	LSF	Reduction %		**Area Red %**			%spread		True Strain
					Per Pass	Cumulative	**Area**	**Per Pass**	**Cumulative**	Per Pass	Cumulative	Per Pass
0	0.15	0.90	0.75				0.11					
1	0.15	0.92	0.75	15716	1.00	1.00	0.11	0.87	0.87	0.13	0.00	0.01
2	0.14	1.01	0.76	31316	8.11	9.03	0.10	6.88	7.70	1.33	1.33	0.08
3	0.12	1.10	0.77	29727	9.19	17.39	0.10	8.06	15.13	1.25	2.60	0.10
4	0.11	1.20	0.78	31377	8.50	24.41	0.09	7.79	21.74	0.78	3.40	0.09
5	0.10	1.31	0.79	30865	8.41	30.77	0.08	7.17	27.35	1.35	4.80	0.09
6	0.09	1.42	0.79	30395	9.18	37.12	0.07	8.49	33.52	0.76	5.60	0.10
7	0.09	1.54	0.80	31553	8.51	42.47	0.07	8.16	38.95	0.38	6.00	0.09
8	0.08	1.71	0.81	33530	10.47	48.49	0.06	9.45	44.72	1.13	7.20	0.11
9	0.07	1.92	0.81	34677	11.69	54.52	0.06	10.70	50.63	1.12	8.40	0.12
10	0.06	2.08	0.82	31249	7.35	57.86	0.05	7.13	54.15	0.25	8.67	0.08
11	0.06	2.26	0.82	30988	9.52	61.87	0.05	9.08	58.31	0.49	9.20	0.10
12	0.05	2.60	0.83	37313	12.28	66.56	0.04	11.21	62.99	1.22	10.53	0.13
13	0.04	2.91	0.84	38901	12.00	70.57	0.04	10.94	67.04	1.20	11.87	0.13
14	0.04	3.30	0.86	41789	9.09	73.24	0.03	7.25	69.43	2.02	14.13	0.10
15	0.04	3.66	0.86	42668	12.50	76.59	0.03	12.19	73.15	0.35	14.53	0.13
16	0.03	4.06	0.87	45866	8.57	78.60	0.03	7.51	75.17	1.16	15.87	0.09
17	0.03	4.43	0.88	46300	12.50	81.27	0.02	11.49	78.02	1.15	17.20	0.13
18	0.03	4.74	0.89	44588	10.71	83.28	0.02	9.70	80.16	1.14	18.53	0.11
19	0.02	5.14	0.89	41265	8.00	84.62	0.02	8.00	81.74	0.00	18.53	0.08
20	0.02	5.47	0.90	38903	8.70	85.95	0.02	7.67	83.14	1.12	19.87	0.09
21	0.02	5.76	0.91	34928	4.76	86.62	0.02	3.70	83.77	1.11	21.20	0.05

Figure 22. Sample A3-24 after Cold Rolling to a Final Thickness of 0.02 in.

The cumulative lateral spread while rolling was approximately 20%, as shown in Figure 23a. The lateral spread was roughly 1−2% per rolling pass (Figure 23b). The increase in LSF can be directly correlated to the lateral spread of the sample. Greater lateral spread, i.e., greater width of the sample, means an increase in the load. Cracks were observed when the reduction was approximately 50% and the sample had a cumulative lateral spread of 8.5%.

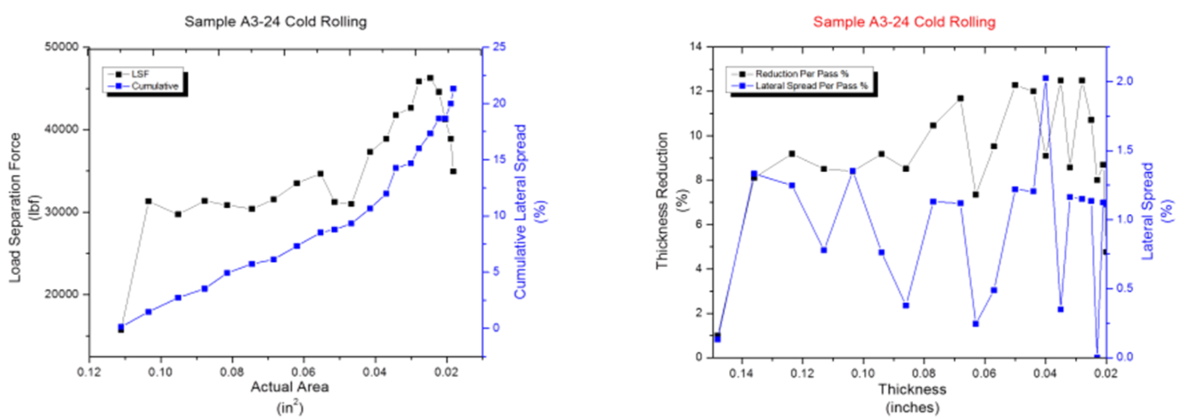

Figure 23. (a) Effect of Cross-Sectional Area on the Cumulative Lateral Spread and LSF; (b) Effect of Thickness on the Lateral Spread per Rolling Pass and Thickness Reduction

Figure 24a is the BSE-SEM image of the longitudinal cross section of the as-rolled sample and a magnified region of the same is shown in Figure 24b. Similar to the PB sample, the carbides fractured perpendicularly to the rolling direction and created voids along the rolling direction. The preexisting porosity was not exacerbated as the rolling progressed. The grains were elongated along the rolling direction and the inhomogeneity in molybdenum concentration was retained.

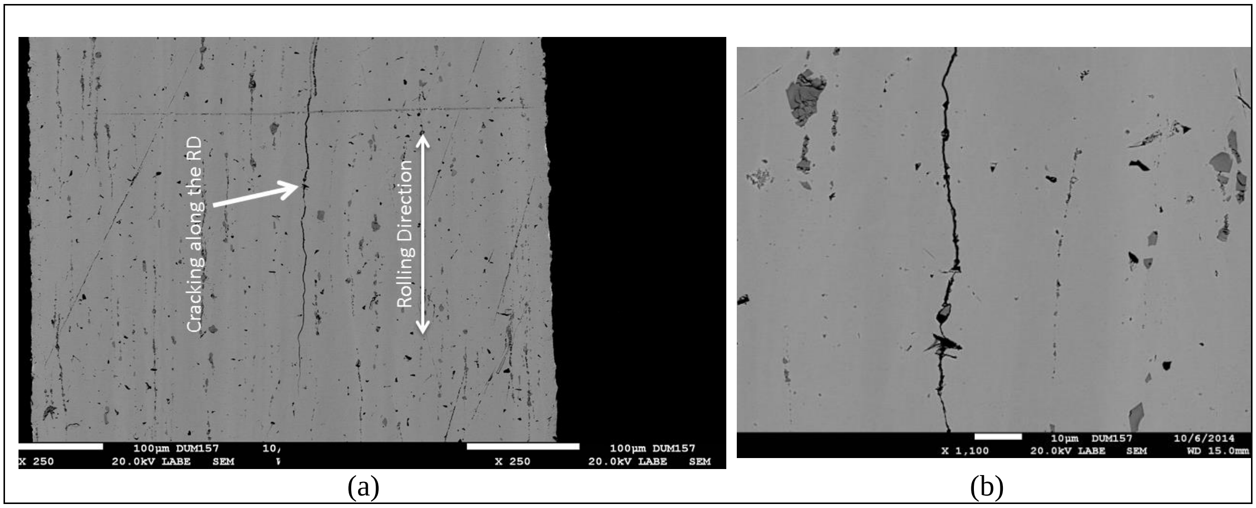

Figure 24. BSE-SEM Images of the Longitudinal Cross Section of the A3-24 Rolled Sample: (a) 250X and (b) further magnified view of the cracked section in (a). (RD = rolling direction).

The samples were later annealed using several durations and temperatures and the microhardness was measured normal to the rolling direction. Below the eutectoid temperature, the hardness was observed to increase drastically, owing to the precipitation of the lamellar phase. However, this contrasts with the hardness increase observed during the homogenization studies. Heat treating the sample above the eutectoid temperature, however, led to a rapid drop in the hardness as the heating time increased.

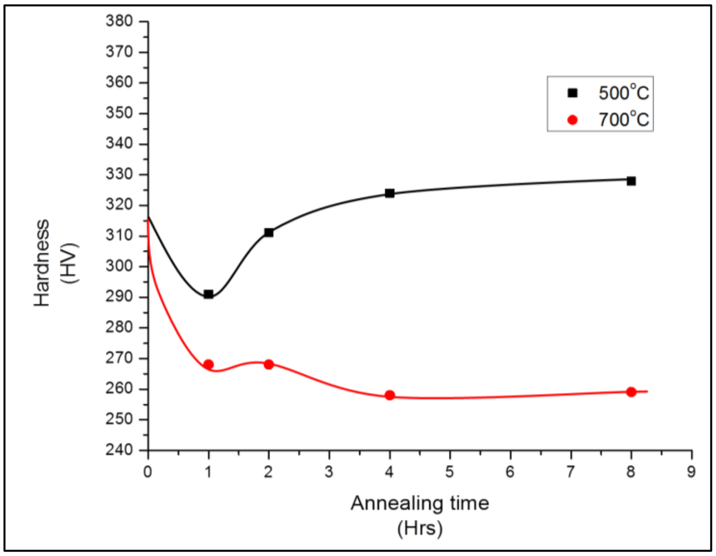

Figure 25. Effect of Annealing the Cold-Rolled A3-24 Samples using Several Durations and Temperatures

To evaluate the consistency of the process, the bottom section of the A3 plate was rolled (Figure 7c). Table 4 shows the rolling data for the A3 plate. After the third rolling pass, the sample temperature increased slightly and after the sixth pass a crack was observed at the rear end of the sample, as shown in Figure 26a. The cumulative lateral spread was roughly between 7% and 9% at the time of cracking (similar to the previous sample). As the rolling progressed, the crack growth was rapid and the tests were stopped before achieving the desired thickness of 0.02 in. The hardness/recovery curves for the sample were not performed because of the premature failure of the sample. An image of the longitudinal cross section of the same (not shown) revealed a microstructure similar to that of sample A3-24. The optical and BSE-SEM images of the crack face are shown in Figure 26b; the BSE-SEM image revealed crack propagation along the molybdenum inhomogeneity banded region or along the carbides (intergranular).

Table 4. Rolling Data to Study the Effect of Location on Cold Rolling: Bottom of the Plate Sample (A3-92), As Cast

Sample A3-92														
				Buck		Reduction		Area Red %			%spread		Stress	True Strain
Pass	Thickness	Length	Width	(Actual)	LSF	Per Pass	Cumulative	Area	Per Pass	Cumulative	Per Pass	Cumulative		Per Pass
0	0.15	0.95	0.75					0.11					0.00	
1	0.13	1.10	0.77	0.03	37141.00	12.03	11.42	0.10	9.08	8.32	3.36	3.49	376836.44	0.13
2	0.11	1.31	0.78	0.02	41921.00	17.97	27.34	0.08	16.90	23.82	1.30	4.84	511855.92	0.20
3	0.09	1.53	0.79	0.02	40051.00	14.29	37.72	0.07	13.08	33.78	1.41	6.32	562593.06	0.15
4	0.08	1.70	0.80	0.02	32742.00	11.11	44.64	0.06	10.10	40.47	1.14	7.53	511593.75	0.12
5	0.07	1.89	0.80	0.02	35372.00	8.75	49.48	0.06	8.41	45.47	0.38	7.93	603422.10	0.09
6	0.07	2.07	0.81	0.02	34325.00	10.96	55.02	0.05	9.85	50.85	1.25	9.27	649541.11	0.12
7	0.06	2.33	0.81	0.02	35594.00	13.85	61.25	0.05	13.85	57.65	0.00	9.27	781804.60	0.15
8	0.05	2.81	0.82	0.01	40885.00	19.64	68.86	0.04	18.95	65.68	0.86	10.22	1107994.58	0.22
9	0.04	3.16	0.83	0.01	35612.00	4.44	70.24	0.04	2.87	66.66	1.65	12.03	993624.53	0.05
10	0.04	3.50	0.84	0.01	31607.00	10.47	73.36	0.03	9.98	69.99	0.54	12.63	979667.11	0.11
11	0.04	3.77	0.84	0.01	32877.00	7.79	75.43	0.03	7.19	72.15	0.66	13.37	1097940.34	0.08
12	0.03	4.08	0.85	0.01	35700.00	9.86	77.85	0.03	9.06	74.67	0.89	14.38	1310957.70	0.10
13	0.03	4.60	0.85		35000.00	10.94	80.28	0.02	10.62	77.36	0.35	14.78	1438021.28	0.12

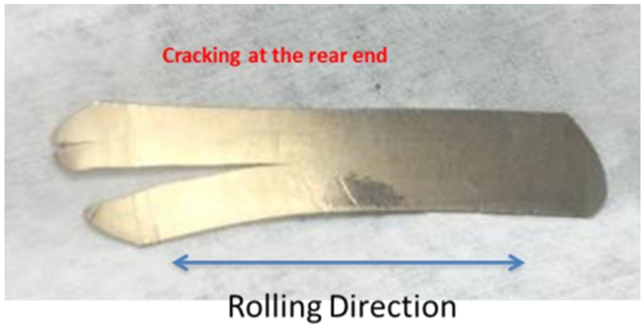

(a)

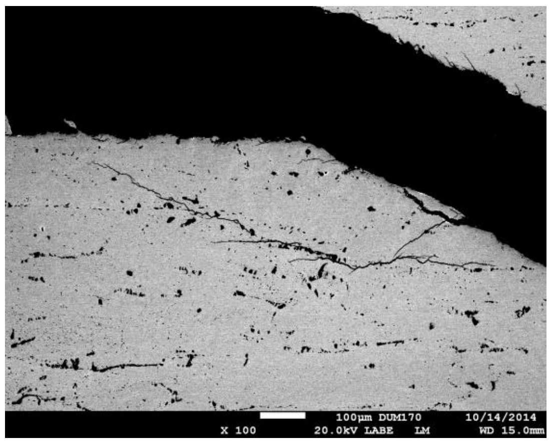

(b)

Figure 26. Sample A3-92 (a) after Cold Rolling; (b) Magnified Region of the Cracked Face

3.3.2.2 Effect of Cold Rolling the Homogenized A3 Samples

Prior to rolling, the samples were homogenized at 900°C for 48 h. The microstructure resulting from this heat treatment is shown in Figure 27. Later the samples were cold rolled from 0.147 in. to 0.02 in., with 10% reduction per rolling pass, using 4 in. rolls, as described previously. No intermediate annealing or trimming of the rolling samples were performed. The current work directly compared the data with the as-cast rolled samples.

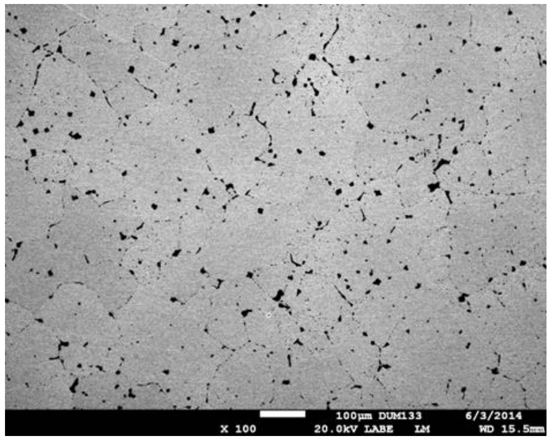

Figure 27. BSE-SEM Image of the Sample Homogenized at 900°C for 48 h

Table 5 shows the cold-rolling data from the top section of the homogenized A3 plate (Figure 27). Slight edge cracking was observed on the seventh rolling pass (highlighted in red in Table 5) as the samples were rolled, but further rolling of the samples resulted in the growth of the cracks. Similar to the previous samples, the crack was observed when the cumulative lateral spread was approximately 7.5%, as shown in Figure 28. Figure 29a shows the sample after achieving a final thickness of 0.025 in. and Figure 29b is the region showing the cracked interface. The cracks propagated through the carbide regions and were intergranular.

Table 5. Rolling Data to Study the Effect of Location on Cold Tolling: Top of the Plate Sample (A3-25), Homogenized at 900°C for 48 h

Sample A3-25 cold rolling													
				Buck		Reduction		**Area Red %**			%spread		True Strai
Pass	Thickness	Length	Width	(Actual)	LSF	Per Pass	Cumulativ	**Area**	**Per Pass**	**Cumulative**	Per Pass	Cumulativ	Per Pass
0	0.15	0.96	0.75					0.11					
1	0.14	1.06	0.76	0.03	30962.00	6.80	6.80	0.10	5.56	5.56	1.33	1.33	0.07
2	0.12	1.16	0.76	0.03	32247.00	10.22	16.33	0.09	9.75	14.76	0.53	1.87	0.11
3	0.11	1.29	0.78	0.03	33931.00	10.57	25.17	0.09	9.28	22.68	1.44	3.33	0.11
4	0.10	1.44	0.78	0.03	36165.00	11.82	34.01	0.08	10.79	31.02	1.16	4.53	0.13
5	0.09	1.60	0.79	0.03	37199.00	10.31	40.82	0.07	9.28	37.42	1.15	5.73	0.11
6	0.08	1.77	0.80	0.03	37363.00	10.34	46.94	0.06	9.55	43.40	0.88	6.67	0.11
7	0.07	1.97	0.81	0.03	37384.00	10.26	52.38	0.06	9.70	48.89	0.63	7.33	0.11
8	0.06	2.19	0.82	0.03	37898.00	10.00	57.14	0.05	8.88	53.43	1.24	8.67	0.11
9	0.06	2.41	0.82	0.03	37732.00	9.52	61.22	0.05	8.75	57.50	0.86	9.60	0.10
10	0.05	2.64	0.83	0.03	39334.00	10.53	65.31	0.04	9.44	61.51	1.22	10.93	0.11
11	0.05	2.90	0.84	0.03	41174.00	9.80	68.71	0.04	9.37	65.12	0.48	11.47	0.10
12	0.04	3.29	0.85	0.03	43318.00	13.04	72.79	0.03	12.00	69.31	1.20	12.80	0.14
13	0.04	3.52	0.85	0.03	45584.00	5.00	74.15	0.03	4.55	70.70	0.47	13.33	0.05
14	0.03	3.81	0.87	0.03	48027.00	10.53	76.87	0.03	8.42	73.17	2.35	16.00	0.11
15	0.03	4.14	0.87	0.03	48831.00	11.76	79.59	0.03	11.56	76.27	0.23	16.27	0.13
16	0.03	4.41	0.87	0.03	51899.00	6.67	80.95	0.02	6.45	77.80	0.23	16.53	0.07
17	0.03	4.72	0.89	0.03	53857.00	7.14	82.31	0.02	5.97	79.13	1.26	18.00	0.07
18	0.03	4.98	0.89	0.03	51095.00	3.85	82.99	0.02	2.98	79.75	0.90	19.07	0.04

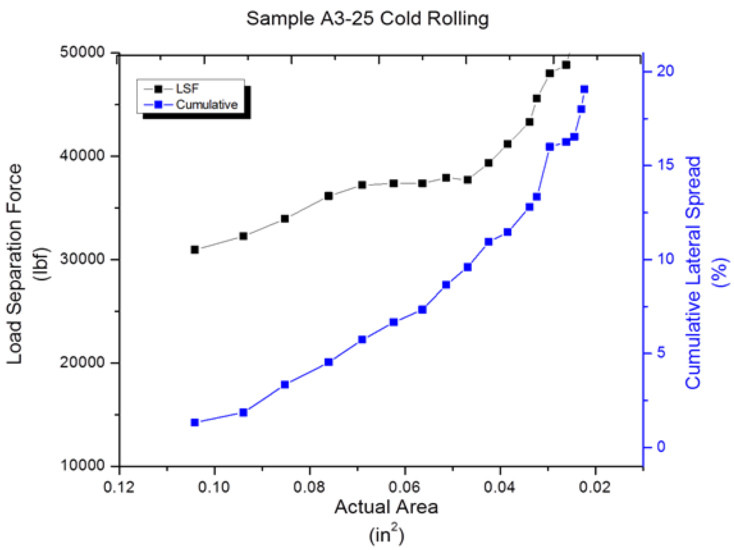

Figure 28. The Effect of Area on the LSF and Cumulative Lateral Spread

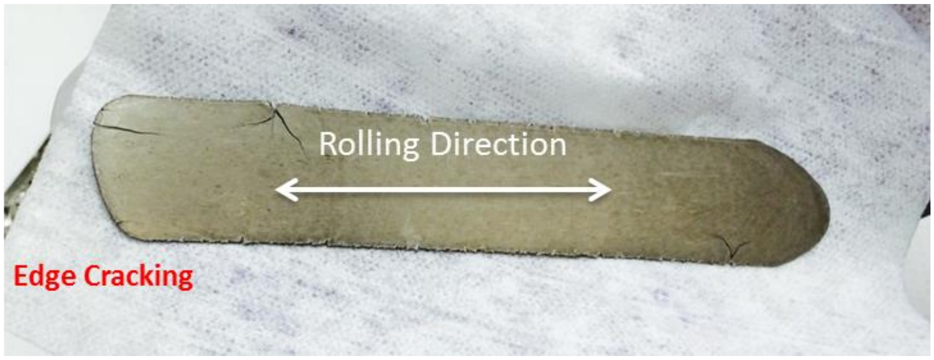

(a)

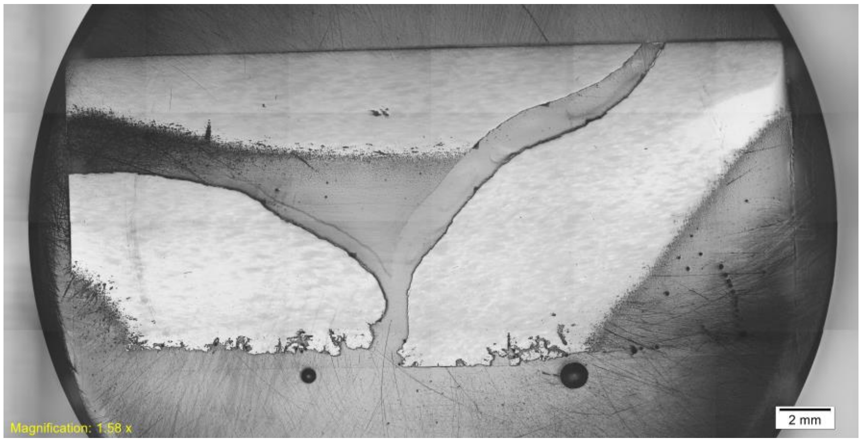

(b)

Figure 29. (a) Sample A3-25 after Cold Rolling and (b) Magnified Region of the Cracked Face

Figure 30a shows the effect of annealing time and temperature on the hardness of the material. Unlike the homogenized samples, these samples showed increased hardness as the homogenization time and temperature increased. Figure 30b is a longitudinal cross-section image of the rolled sample. The rolling resulted in a decrease of the grain size by approximately four times in the direction perpendicular to the rolling. This may have been the primary cause of the precipitation of the lamellar phase, as shown in Figure 31a. Compared to the microstructure of the 500°C-2 h annealed sample (Figure 31a), the 700°C-2 h annealed sample (Figure 31b) microstructure is fairly clean and does not contain any lamellar precipitates. The evidence of precipitation becomes more evident when the annealing time is increased to 8 h. No precipitation is observed in the 700°C-8 h annealed sample (Figure 31d), whereas in the 500°C-8 h annealed sample (Figure 31c), the precipitation is more pronounced.

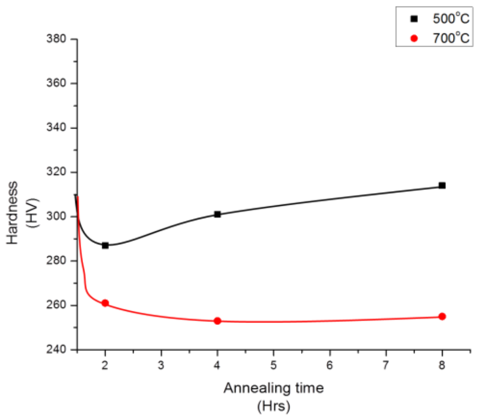

(a)

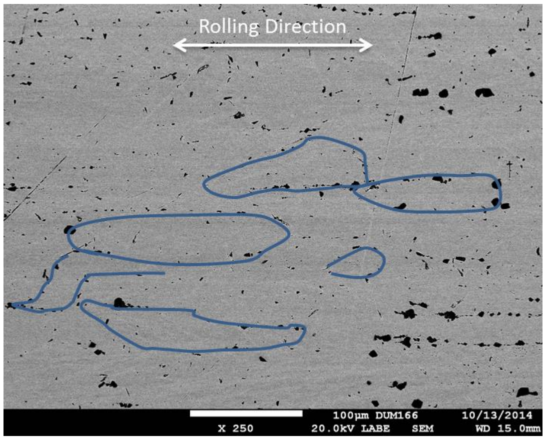

(b)

Figure 30. (a) Effect of Annealing the Cold-Rolled A3-25 Samples at Several Times and Temperatures; (b) BSE-SEM Image of the Longitudinal Cross Section Showing the Grains (in blue lines)

The bottom sample behaved similarly to the top section of the A3-25 sample and the crack propagated through the edges. Because of the similarity of results with A3-25, these samples are not further discussed.

Based on these studies, one can conclude that cold rolling of both homogenized and non-homogenized samples propagates the existing porosity, elongates the grains along the rolling direction, fractures the carbides, and leaves porosity behind. The kinetics of phase transformation at sub-eutectoid temperatures is similar to that of the unstrained materials and stress relief occurs immediately upon annealing.

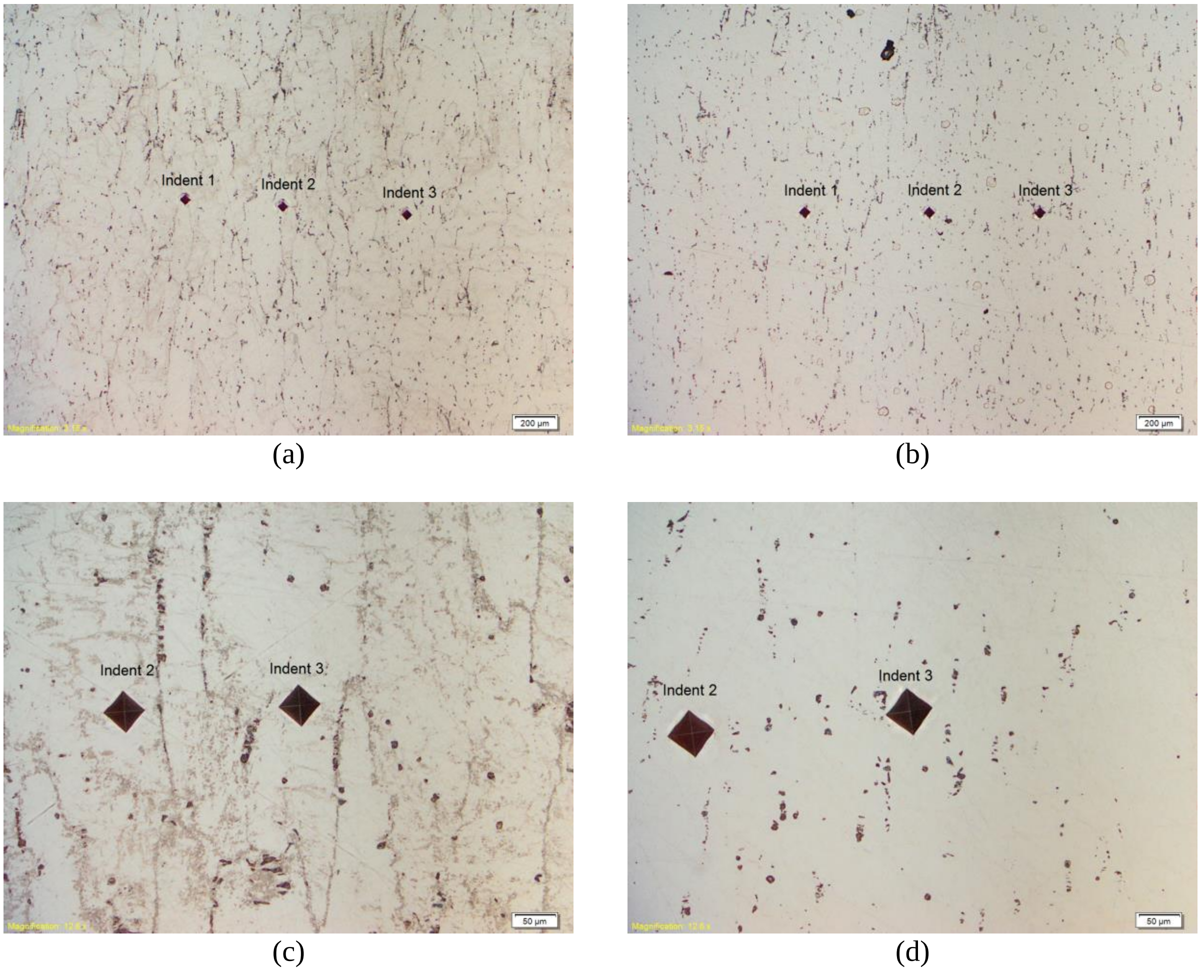

Figure 31. Optical Images of a Normal Section of the A3-25 Rolled Sample after Annealing: (a) at 500°C for 2 h, (b) at 700°C for 2 h, (c) at 500°C for 8 h, (d) at 700°C for 8 h. Images (a) and (c) on the left show precipitation of the lamellar phase at the grain boundaries for comparison with (b) and (d), respectively, on the right. Comparison of images in the top row with those directly below shows the effects of annealing time.

3.3.2.3 Effect of Hot Rolling the As-Cast A3 Samples

As-cast A3 samples were hot rolled from 0.147 in. to 0.02 in. with 15% reduction per rolling pass using 4 in. rolls at 650°C, as described previously. The samples were cooled, measured for their dimensions, and then later heated at 650°C for 20 min before rolling.

Table 6 presents the hot-rolling data generated after rolling the top of the as-cast A3-23 sample. Figure 32a shows the as-rolled sample. Slight edge cracking was noticed while rolling the sample, but no significant cracks were observed. The cumulative lateral spread was similar to that of the cold-rolled sample and was ~22%. The LSF was approximately 25,000 lb, in contrast to 35,000 lb observed while rolling cold with much smaller reductions. Figure 32b shows the effect of LSF as a function of cross-sectional area and cumulative lateral spread. As the sample area decreased, the lateral spread increased, causing a slight increase in LSF.

Table 6. Rolling Data to Study the Effect of Location on Hot Rolling: Top of the Plate Sample (A3-23), As Cast

Sample A3-23 Hot Rolling at 650C														
				Buck		Reduction		**Area Red %**			%spread		Lsf/area	True Strain
Pass	Thickness	Length	Width	(Actual)	LSF	Per Pass	Cumulativ	**Area**	**Per Pass**	**Cumulative**	Per Pass	Cumulative		Per Pass
0.00	0.15	0.90	0.75	0.00				0.11					0.00	
1.00	0.12	1.10	0.78	0.02	22201.00	16.33	16.33	0.10	13.54	13.54	3.33	3.33	232897.98	0.18
2.00	0.10	1.31	0.78	0.02	23143.00	16.26	29.93	0.08	15.61	27.04	0.77	4.13	287694.39	0.18
3.00	0.09	1.51	0.80	0.02	21455.00	16.50	41.50	0.07	14.69	37.75	2.18	6.40	312627.50	0.18
4.00	0.07	1.85	0.81	0.02	20969.00	15.12	50.34	0.06	13.95	46.43	1.38	7.87	355063.75	0.16
5.00	0.06	2.17	0.82	0.02	21140.00	17.81	59.18	0.05	16.59	55.32	1.48	9.47	429151.44	0.20
6.00	0.05	2.63	0.82	0.02	21913.00	20.00	67.35	0.04	19.71	64.13	0.37	9.87	554030.14	0.22
7.00	0.04	3.13	0.84	0.02	23738.00	12.50	71.43	0.04	11.12	68.11	1.58	11.60	675257.44	0.13
8.00	0.04	3.58	0.85	0.02	23165.00	11.90	74.83	0.03	10.33	71.41	1.79	13.60	734836.95	0.13
9.00	0.03	3.92	0.88	0.02	24605.00	13.51	78.23	0.03	10.87	74.52	3.05	17.07	875747.44	0.15
10.00	0.03	4.60	0.89	0.02	30722.00	15.63	81.63	0.02	14.86	78.30	0.91	18.13	1284257.17	0.17
11.00	0.02	5.21	0.90	0.02	27830.00	11.11	83.67	0.02	9.71	80.41	1.58	20.00	1288425.93	0.12
12.00	0.02	5.95	0.92	0.02	32829.00	12.50	85.71	0.02	11.04	82.57	1.67	22.00	1708508.98	0.13

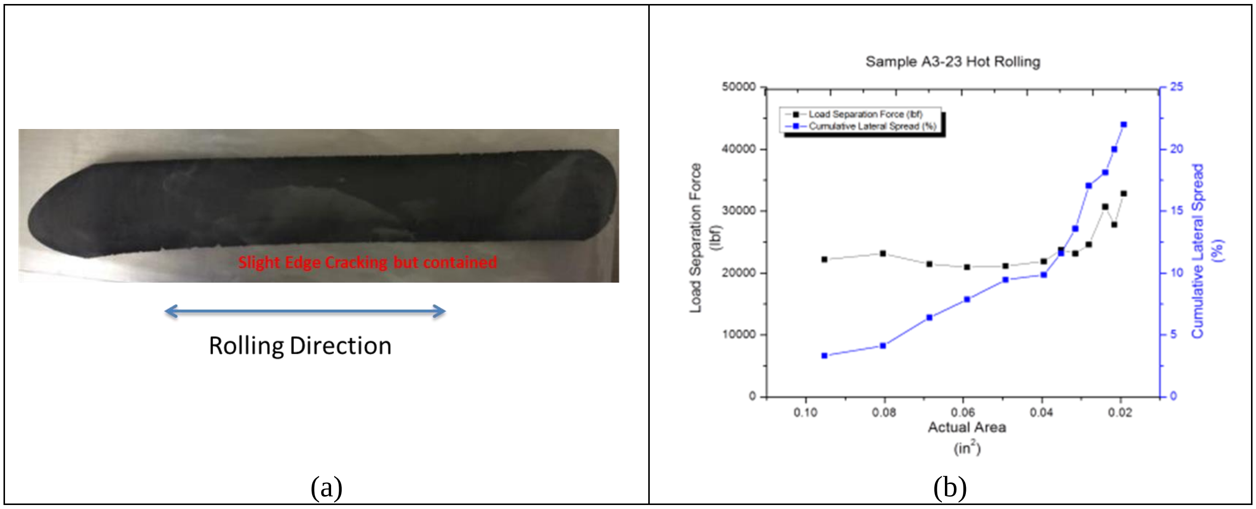

Figure 32. (a) As-Cast U-10Mo Sample after Hot Rolling at 650°C; (b) Effect of Cross-Sectional Area on the LSF and Cumulative Lateral Spread

Figure 33a presents a longitudinal cross-sectional image of the hot-rolled sample. One can observe that the molybdenum inhomogeneity is retained upon rolling the as-cast sample and is more pronounced than in the cold-rolled samples. The carbides did not fracture and the porosity from the castings was no longer visible. The grain boundaries were difficult to discern; using techniques such as electron backscatter diffraction will be better for discerning grain boundaries. Annealing the samples at 500°C resulted in a drastic increase in hardness compared to the cold-rolled samples. Figure 34a presents the optical image of the sample that was annealed at 500°C for 2 h; it reveals the precipitation of the lamellar phase in the molybdenum-lean regions. The precipitation was prominent along the grain boundaries and revealed the grain size to be 25−30 μm. Hot rolling significantly refined the grain size, as previously observed in Figure 13. The increase in hardness can be attributed to large-scale precipitation of the lamellar phase. This becomes clearer in a comparison of Figure 34a with Figure 34c. The volume fraction of the lamellar phase precipitated after 2 h at 500°C is greater than in the sample annealed for 8 h at the same temperature. Annealing the samples above the eutectoid temperature produced conditions similar to those for the cold-rolled samples, and the samples were relieved of the stress immediately (Figure 33b).

The microstructure of the samples annealed above the eutectoid temperature (Figure 34b and d) was clearer than that of the samples annealed below it (Figure 34a and c). Similar experiments with the bottom section yielded similar results and are discussed here.

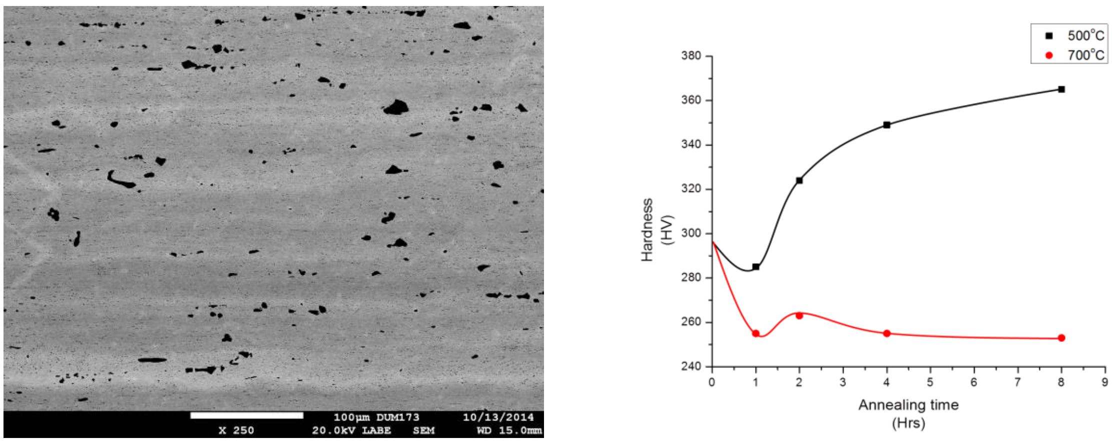

(a) (b)

Figure 33. (a) BSE-SEM Image of the Longitudinal Cross Section of the Hot-Rolled Sample; (b) Recovery Curve of the Hot-Rolled Sample

The results corroborate the previous hot-rolling single-pass experiments well. Hot rolling significantly reduces the grain size and this may be due to DRX. Further systematic studies may be needed to validate this hypothesis. It is interesting to note that hot reduction was able to eliminate the casting defects but unable to homogenize the sample. As was previously observed by Joshi et al. (2014), strain had a significant effect on homogenization. Microstructure-based modeling/EDS line scan studies need to be conducted to determine the degree of homogeneity achieved via this process and a solution may be identified to homogenize the material without performing an energy-intensive homogenization heat treatment. However, the refined grain size may be useful in expediting homogenization.

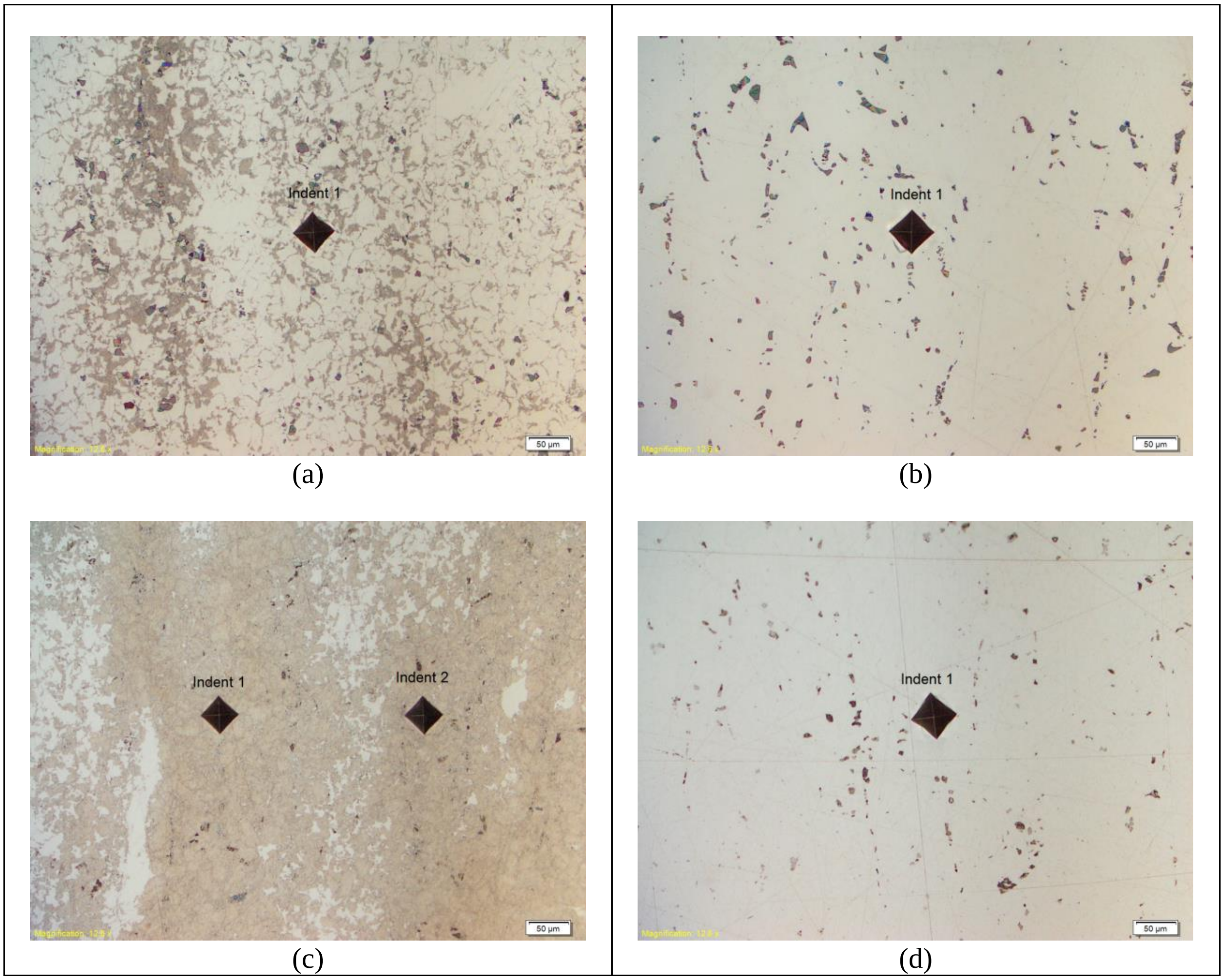

Figure 34. Optical Images of the Normal Section of the A3-23 Rolled Sample after Annealing: (a) at 500°C for 2 h, (b) at 700°C for 2 h, (c) at 500°C for 8 h, and (d) at 700°C for 8 h. Images (a) and (c) on the left show precipitation of the lamellar phase at the grain boundaries below the eutectoid temperature in comparison with (b) and (d) on the right, respectively. Comparison of images in the top row with those directly below shows the effects of annealing time.

3.3.2.4 Effect of Hot Rolling the Homogenized A3 Samples

A set of samples was homogenized at 900°C for 48 h prior to hot rolling. A rolling schedule similar to that described in Section 3.3.2.3 was used. Table 7 indicates the effect of rolling on the mill LSF and sample dimensions. No cracks were observed (Figure 35a) during the rolling and similar to previous samples, the lateral spread was large in these samples. The load increase (Figure 35b) can be attributed to the increase in the spread of the samples.

Table 7. Rolling Data to Study the Effect of Location on Hot Rolling: Top of the Plate Casting (A3-22) As-Cast

Sample A3-22 Hot rolling													
				Buck		Reduction		**Area Red %**			%spread		True Strain
Pass	Thickness	Length	Width	(Actual)	LSF	Per Pass	Cumulative	**Area**	**Per Pass**	**Cumulative**	Per Pass	Cumulative	Per Pass
0	0.15	0.91	0.75					0.11					
1	0.12	1.10	0.77	0.02	20033.00	18.24	17.69	0.09	16.61	16.04	2.00	2.00	0.20
2	0.10	1.32	0.78	0.18	20994.00	14.88	29.93	0.08	13.21	26.84	1.96	4.00	0.16
3	0.08	1.58	0.78	0.13	20948.00	19.42	43.54	0.07	19.00	40.74	0.51	4.53	0.22
4	0.07	1.92	0.80	0.02	23098.00	15.66	52.38	0.06	13.83	48.94	2.17	6.80	0.17
5	0.06	2.28	0.81	0.02	23387.00	18.57	61.22	0.05	17.66	57.95	1.12	8.00	0.21
6	0.05	2.79	0.82	0.02	25175.00	17.54	68.03	0.04	16.53	64.90	1.23	9.33	0.19
7	0.04	3.37	0.83	0.02	25870.00	14.89	72.79	0.03	13.65	69.69	1.46	10.93	0.16
8	0.03	3.90	0.85	0.02	23896.00	15.00	76.87	0.03	13.67	73.84	1.56	12.67	0.16
9	0.03	4.33	0.86	0.02	23496.00	11.76	79.59	0.03	10.72	76.64	1.18	14.00	0.13
10	0.03	4.77	0.87	0.02	22186.00	10.00	81.63	0.02	8.95	78.73	1.17	15.33	0.11
11	0.02	5.75	0.89	0.02	29779.00	22.22	85.71	0.02	20.42	83.08	2.31	18.00	0.25

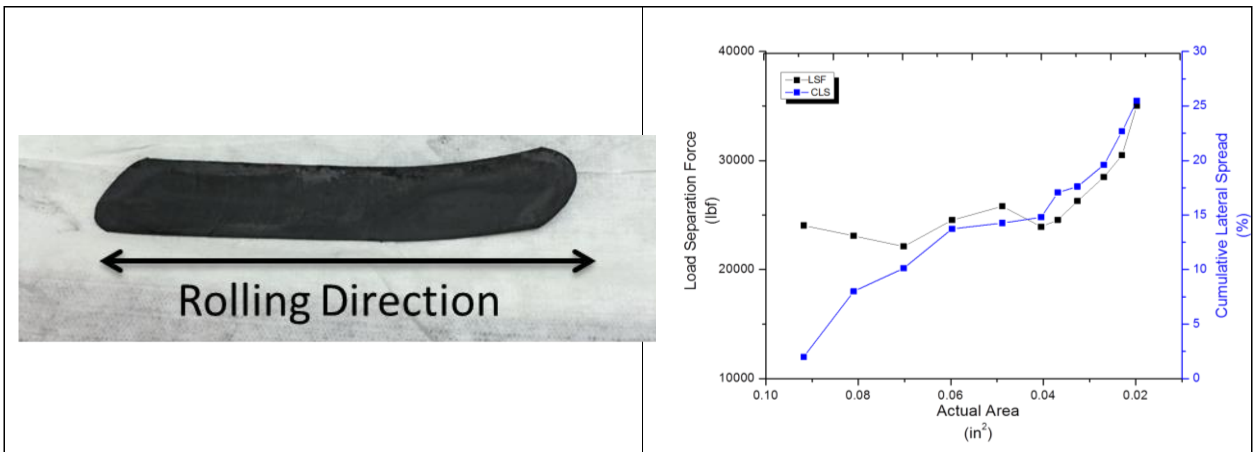

(a) (b)

Figure 35. (a) As-Cast U-10Mo Sample after Hot Rolling at 650°C; (b) Effect of Cross-Sectional Area on the LSF and Cumulative Lateral Spread

Figure 36a presents the longitudinal cross-section image of the as-rolled sample. No chemical banding was observed in these samples and the carbides did not deform perpendicularly to the rolling directions. Grain boundaries were not discernable in these microstructures. The samples were later annealed at 500 and 700°C to determine the recovery curves (Figure 36b). Annealing immediately relieved the residual stress in these samples and remained constant in the case of the 700°C samples, whereas the hardness increased linearly with annealing time in the case of the 500°C samples.

The microstructures of the annealed samples in the normal direction observed under an optical microscope revealed the precipitation of the lamellar phase in the 500°C samples (Figure 36a and Figure 37a). The rolling had caused refinement of the grains and as the annealing time at 500°C increased, the increased precipitation of the lamellar phase caused an increase in the hardness (Figure 36b). The precipitation of the lamellar phase is prominent along the grain boundaries and reveals them distinctly. Samples annealed at 700°C (Figure 36b and Figure 37b) were entirely gamma phase and no other precipitates were observed.

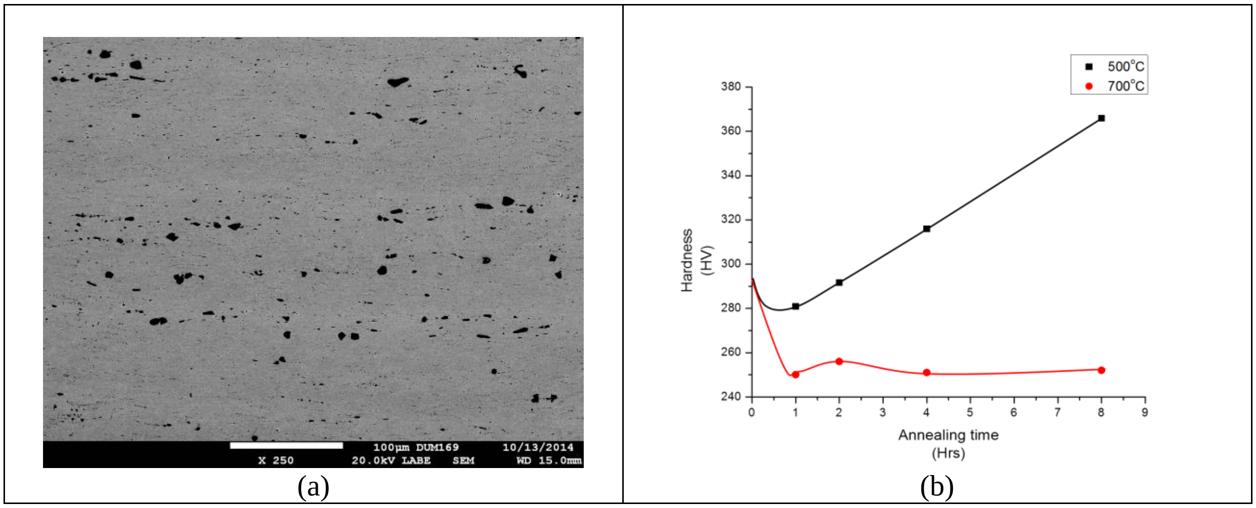

(a) (b)

Figure 36. (a) BSE-SEM Image of the Longitudinal Cross Section of the Hot-Rolled Sample; (b) Recovery Curve of the Hot-Rolled Sample

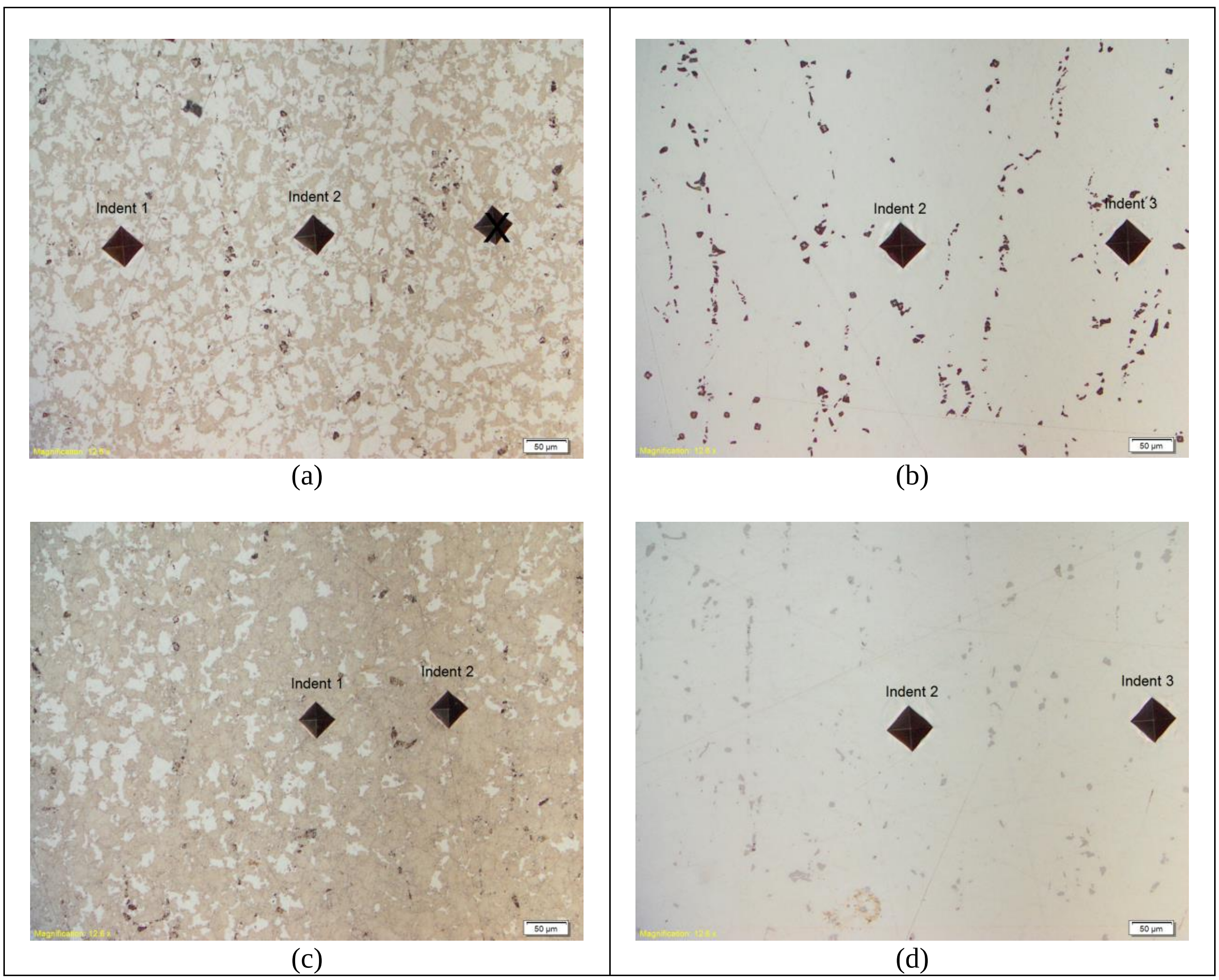

(a) (b) (c) (d)

Figure 37. Optical Images of the Normal Section of the A3-22 Rolled Sample after Annealing: (a) at 500°C for 4 h, (b) at 700°C for 4 h, (c) at 500°C for 8 h, and (d) at 700°C for 8 h. Images (a)

and (c) on the left show precipitation of the lamellar phase at the grain boundaries for comparison with (b) and (d) on the right, respectively. Comparison of images in the top row with those directly below shows the effects of annealing time.

4.0 Discussion

Despite the three different sets of materials used in the current work, the results can primarily be divided into the effects of hot and cold rolling of the as-cast and the homogenized samples. Examination of sample cracking,

In all these samples it was noteworthy that the lateral spread in each sample was approximately 20% when rolled to a final thickness of 0.02 in. Any cracking observed was initiated between 5 and 10% of the lateral spread. Table 8 summarizes the effects of hot and cold rolling the 0.2 in. interrupted rolling A3 sample.

Table 8. Effects of Hot and Cold Rolling the 0.2 in. Interrupted Rolling A3 Sample

Initial Condition	Rolling	Region	Sample ID	Crack location	# of Passes before crack was Observed	Cumulative Lateral Spread at crack initiation	Total lateral Spread
As Cast	Hot rolling	Top	A3-23	Edge	7	22	22
		Bottom	A3-96	Edge and Tail end	7	22.	35
	Cold Rolling	Top	A3-24	Edge (contained)	9	8.5	21
		Bottom	A3-92	Tail end	6	9.2	14
As Cast and Homogenized	Hot rolling	Top	A3-22	NA	-	-	18
		Bottom	A3-98	NA	-	-	25
	Cold Rolling	Top	A3-25	Edge	7	7.3	19
		Bottom	A3-97	Edge	14	18	18

Cracks initiated along the rolling direction usually propagated rapidly as the number of passes increased (see Figure 15, Figure 21, and Figure 24). The cracks perpendicular to the rolling direction were either restricted or transverses along the rolling direction as the number of passes increased. The cracks were usually initiated at preexisting porosity or carbide locations (Figure 26a and Figure 29b). The probability of cracking in cold rolling the samples (both as-cast and homogenized) was greater because rolling was ineffective in curing the as-cast defects. Cracks were consistently observed in the as-rolled material, consistent with the initial porosity within the as-cast sample. Hot rolling was effective in eliminating the initial casting defects as the number of passes increased, in contrast to the cold rolling.

Cold rolling also led to the fracture of carbides perpendicular to the rolling direction (Figure 15, Figure 21, and Figure 24). Similar observations were also made by the current authors during the compression tests (Nyberg et al. 2013; Joshi et al. 2014a b). Based on the work done by Tabei and Garmestani (2013), it was determined that the state of stress in the materials accompanied by the high strength of the matrix leads to fracture of the carbides. The fractured carbides, upon further rolling, created porosity between the two particles and the rolling loads/reductions were not enough to close the pores (Figure 24). The additional cold rolling of both the homogenized and as-cast samples led to further separation of the fractured carbides. Hot rolling was beneficial in avoiding the fracture of the carbides, in contrast to cold rolling. Molybdenum inhomogeneity in the as-cast material was responsible for development of a fibrous texture (Mo-rich and -lean regions) in both cold- and hot-rolled samples, which may have also caused the residual stresses and eventual failure of the samples.

Further investigation needs to be done to prevent the lateral spread of the material during rolling, but this work provides a baseline for the modeling studies. In this study, it was observed that the lateral spread combined with cold rolling of the as-cast samples and the development of the fibrous texture made the samples more susceptible to cracking/failure. The current FEM models assume no lateral spread in the material and the incorporation of lateral spread is expected to yield beneficial results.

To determine mill parameters such as coefficient of friction, flow stress, and LSF during cold rolling, classical equations (Equations 4–6) of rolling (Dieter 1976) were used to plot the graph shown in Figure 38.

$$P = \frac{2}{\sqrt{3}}\sigma_o\left[\frac{1}{Q}(e^Q - 1)b\sqrt{R\Delta h}\right] \tag{4}$$

where P is the rolling load/LSF, σ_o is the flow stress, R is the roll radius, and Δh is the draft/ buck; Q and its constituent, L_p, are given by the equations

$$Q = \frac{\mu L_p}{\bar{h}} \tag{5}$$

$$L_p = \sqrt{R\Delta h} \tag{6}$$

where μ is the coefficient of friction, L_p is the projected length of contact, and $\bar{h}$ is the mean thickness between entry and exit from the rolls.

The model uses 10% reduction for the first pass and the LSF for that pass is highlighted in red in Figure 38. It was determined that the flow stress during the initial cold-rolling 10% pass was roughly 180 ksi and the coefficient of friction was predicted to be between 0.4 and 0.6.

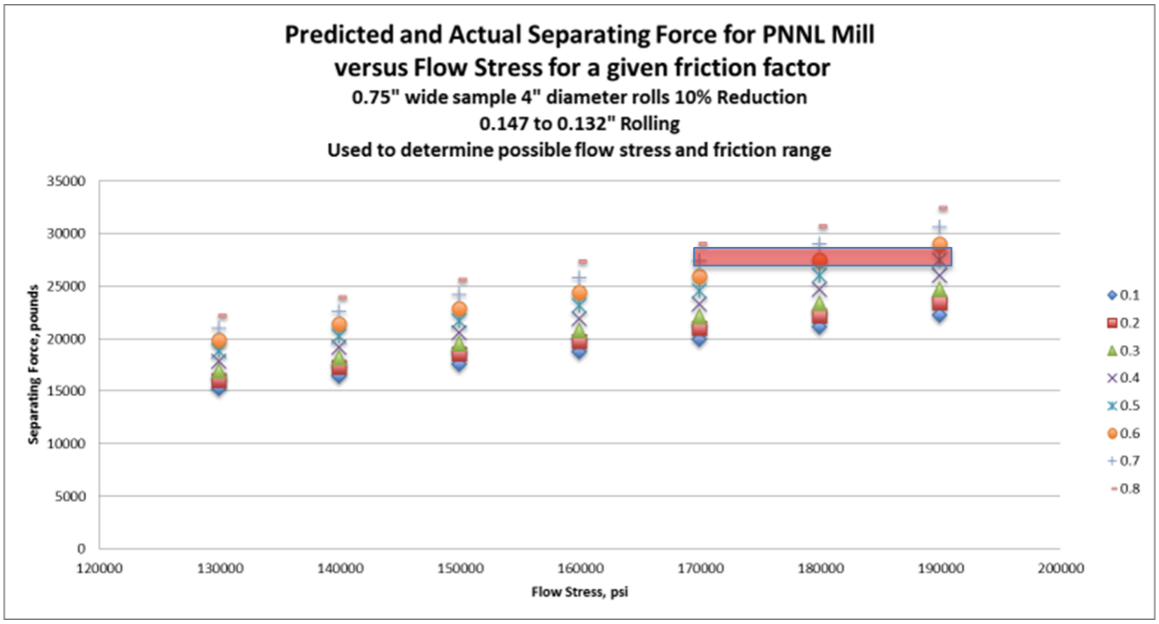

Figure 38. Actual LSF of the PNNL Mill and That Predicted Using a Classical Equation to Determine the Approximate Coefficient of Friction (μ) of the Rolls and Flow Stress of U-10Mo During Rolling. The region highlighted in red is the experimental calculation.

The rolling data was then used to feed the FEM models and was used to predict the LSF for the PNNL mills (Figure 39a and b). The modeling results seem to be in good agreement with the measured ones. The details of this study have been mentioned in the modeling report (Soulami et al. 2014).

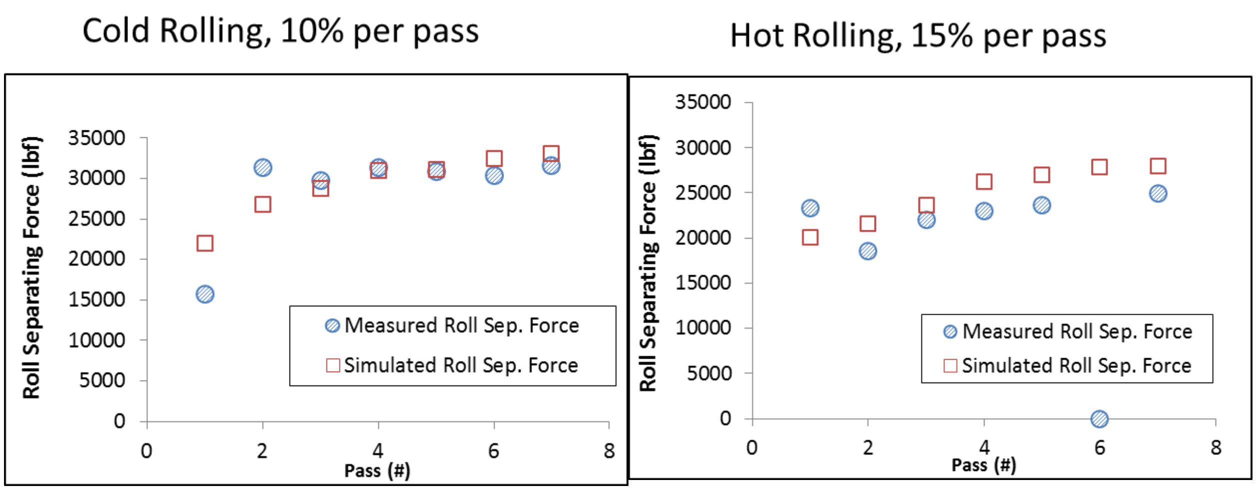

(a) (b)

Figure 39. Experimental and Simulated LSF as a Function of Number of Passes with a coefficient of friction of 0.4.

Cold rolling the as-cast and homogenized material elongated the grain along the rolling direction and formed pancake-like structures. For an eventual thickness of 0.02 in., the grains had aspect ratios of over 10:1 in certain cases (Figure 30, Figure 31). The large grain sizes, upon annealing, were less susceptible to precipitation of the lamellar phase. No recrystallization was observed upon annealing; however, the recovery/stress relief was drastic in both the as-cast and homogenized samples. Annealing the samples in the sub-eutectoid regime was responsible for the precipitation of the lamellar phase and led to an increase in the hardness.

The hot rolling was ineffective in eliminating the molybdenum inhomogeneity and formed a pronounced banded or fibrous texture. Hot rolling, in contrast to cold rolling, resulted in significant grain refinement due to DRX. A cumulative strain of over 50% was essential to the DRX of the samples. This was more pronounced in the single-pass experiments (Section 3.2). This phenomenon was common to both as-cast and homogenized as well as single- and multiple-pass experiments. The results can be corroborated with the hot compression testing data (Nyberg et al. 2013; Joshi et al. 2014), which showed a broad peak (see Figure 40a) after attaining the yield stress (Rollett et al. 2004). To determine the degree of recrystallization, systematic electron backscatter diffraction analysis needed to be conducted on the as-rolled samples. The grain sizes of the recrystallized samples were approximately 25 μm after hot rolling from 0.2 in. to 0.02 in. Annealing the recrystallized samples led to rapid precipitation of the lamellar phase and increased hardness, as shown in Figure 41.

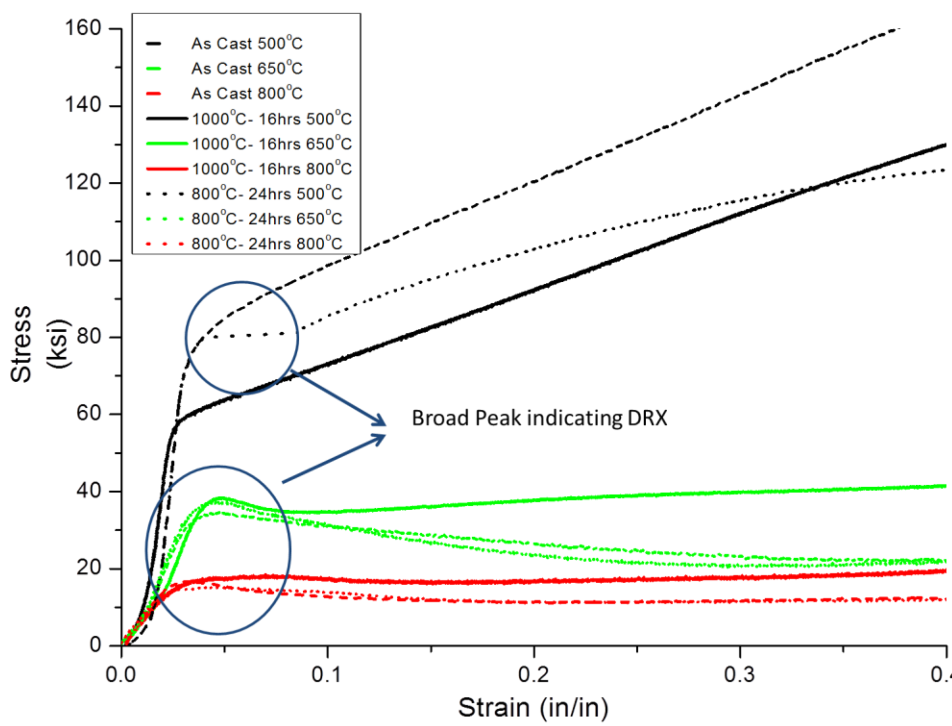

Figure 40. Effect of Temperature on Results of Compression Testing of U-10Mo. Broad peaks indicate DRX.

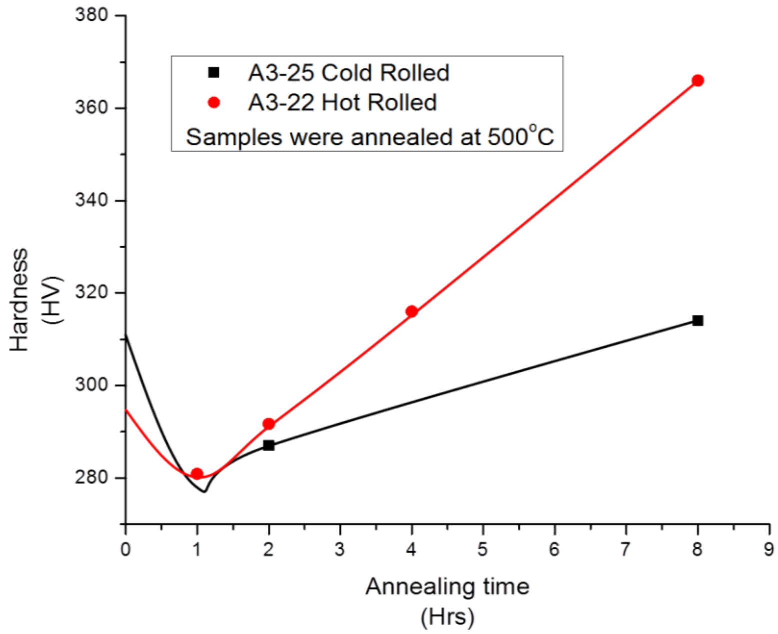

Figure 41. Hardness of the Homogenized and Later Hot-Rolled or Cold-Rolled Samples after Annealing at 500°C

5.0 Conclusions

U-10Mo samples were subjected to hot and cold rolling schedules to determine the effects on the resulting microstructure and recovery curves. The following observations were derived from the study:

1. More than 50% reduction during hot rolling in the gamma phase field causes DRX of the grains and results in a refined microstructure.
2. Hot rolling is beneficial in eliminating the casting defects and does not fracture the carbides.
3. Both hot and cold rolling as-cast samples retains the molybdenum inhomogeneity in the form of a banded microstructure, whereas homogenization heat treatment completely eliminates these issues.
4. A refined grain size causes rapid precipitation of the lamellar phase and results in increased hardness. This is typically observed in hot rolled samples where recrystallization caused grin refinement.
5. Annealing in the gamma phase field relieves the stress in the sample effectively without greatly affecting the grain size or the as-rolled microstructure.
6. Cold rolling, in contrast to hot rolling, does not cause grain refinement. The grains look more pancake shaped than equiaxed indicating no recrystallization, however annealing the same above the eutectoid temperature causes grain refinement.
7. Cold rolling causes the fracture of the carbides and is inefficient in closing the casting defects and hence it is recommended to hot roll the material to eliminate the casting porosity before initiating any cold rolling.

6.0 Future Work

1. Experimentally verify the initiation of DRX and the ways to tailor the grain size.
2. Complete the studies of combinations of cold and hot rolling and annealing to investigate the microstructure development.
3. Study the effect of mill parameters on the lateral spread.
4. Investigate the effects of rolling texture on the precipitation of the lamellar phase and ways to mitigate them.

7.0 References

Burkes D and D Senor. 2014. *The Fuel Fabrication Capability and Uranium-molybdenum Alloy: An Overview*. Presented at 2014 TMS Annual Meeting & Exhibition San Diego, California, USA.

Burkes DE, T Hartmann, R Prabhakaran, and J-F Jue. 2009. "Microstructural characteristics of DU–xMo alloys with x = 7–12 wt%." *Journal of Alloys and Compounds* 479(1–2):140−147.

Burkes DE, R Prabhakaran, T Hartmann, J-F Jue, and FJ Rice. 2010. "Properties of DU–10 wt% Mo alloys subjected to various post-rolling heat treatments." *Nuclear Engineering and Design* 240(6):1332−1339.

Dieter GE. 1976. *Mechanical Metallurgy*. McGraw-Hill.

Edwards DJ, RM Ermi, A Schemer-Kohrn, NR Overman, JC Henager, D Burkes. 2012. *Characterization of U-Mo Foils for AFIP-7*. PNNL-21990, Pacific Northwest National Laboratory, Richland, Washington.

Ginzburg VB. 1993. *High-Quality Steel Rolling: Theory and Practice*. Taylor & Francis, USA.

Joshi VV, EA Nyberg, CA Lavender, D Paxton, H Garmestani and DE Burkes. 2013. "Thermomechanical Process Optimization of U-10 wt% Mo – Part 1: High-Temperature Compressive Properties and Microstructure." *Journal of Nuclear Materials*. Available online at http://dx.doi.org/10.1016/j.jnucmat.2013.10.065

Joshi VV, EA Nyberg, CA Lavender, D Paxton, and DE Burkes. 2014. "Thermomechanical Process Optimization of U-10wt% Mo – Part 2: The Effect of Homogenization on the Mechanical Properties and Microstructure." *Journal of Nuclear Materials* 465:710-718.

Nyberg E, V Joshi, C Lavender, D Paxton, and D Burkes. 2013a. *The Influence of Casting Conditions on the Microstructure of As-Cast U-10Mo alloys: Characterization of the Casting Process Baseline*. PNNL-23049, Pacific Northwest National Laboratory, Richland, Washington.

Nyberg EA, VV Joshi, CA Lavender, D Paxton, and D Burkes. 2013b. *The Influence of Homogenization on the Mechanical Properties and Microstructure on U-10Mo Alloy*. PNNL-23348, Pacific Northwest National Laboratory, Richland, Washington.

Park Y, J Yoo, K Huang, DD Keiser Jr, JF Jue, B Rabin, G Moore, and YH Sohn. 2014. "Growth kinetics and microstructural evolution during hot isostatic pressing of U-10 wt.% Mo monolithic fuel plate in AA6061 cladding with Zr diffusion barrier." *Journal of Nuclear Materials* 447(1–3):215−224.

Park Y, DD Keiser Jr, and YH Sohn. 2015. "Interdiffusion and reactions between U–Mo and Zr at 650 °C as a function of time." *Journal of Nuclear Materials* 456(0):351−358.

Perez E, B Yao, DD Keiser Jr, and YH Sohn. 2010. "Microstructural analysis of as-processed U–10 wt.%Mo monolithic fuel plate in AA6061 matrix with Zr diffusion barrier." *Journal of Nuclear Materials* 402(1):8−14.

Rollett A, FJ Humphreys, and GS Rohrer. 2004. *Recrystallization and Related Annealing Phenomena*. Elsevier Science.

Senor DJ and D Burkes. 2014. *Fuel Fabrication Capability Research and Development Plan Global Threat Reduction Initiative – Convert Program*. PNNL-22528, Pacific Northwest National Laboratory, Richland, Washington.

Soulami A, CA Lavender, D Paxton, and D Burkes. 2014. *Rolling Process Modeling Report: Finite Element Prediction of Roll Separating Force and Rolling Defects*. PNNL-23313, Pacific Northwest National Laboratory, Richland, Washington.

Tabei A and H Garmestani. 2013. *Precipitate Refinement in Thermomechanical Processing of Dual Phase Alloys*. Georgia Institute of Technology, Atlanta, Georgia.

Vergara H, Kim D and Wiliams K. 2014, *Industrial Engineering Support for Low-Enriched Uranium Fuel Fabrication Process Flow –Task 1.* Oregon State University, Corvaillis, Oregon

Vergara H, Kim D and Wiliams K. 2014, *Industrial Engineering Support for Low-Enriched Uranium Fuel Fabrication Process Flow –Task 2.* Oregon State University, Corvaillis, Oregon

Pacific Northwest
NATIONAL LABORATORY

Proudly Operated by **Battelle** *Since 1965*

U.S. DEPARTMENT OF
ENERGY

902 Battelle Boulevard
P.O. Box 999
Richland, WA 99352
1-888-375-PNNL (7665)
www.pnnl.gov